Author Manuscript

Author Manuscript

Author Manuscript

Author Manuscript

HHS Public Access

Author manuscript

ACS Nano. Author manuscript; available in PMC 2022 March 23.

Published in final edited form as:

ACS Nano. 2021 March 23; 15(3): 4728–4746. doi:10.1021/acsnano.0c09254.

A High-Throughput Screening Platform for Nanoparticle-Mediated Alterations of DNA Repair Capacity

Sneh M Toprani[#a], **Dimitrios Bitounis**[#b], **Huang Qiansheng**[b,c], **Nathalia Oliveira**[b], **Kee Woei Ng**[b,d,e], **Chor Yong Tay**[d,f], **Zachary D Nagel**[a,¥], **Philip Demokritou**[b,¥]

[a]John B Little Center of Radiation Sciences, Department of Environmental Health, Harvard T H Chan School of Public Health, Boston, Massachusetts 02115, United States

[b]Center for Nanotechnology and Nanotoxicology, Department of Environmental Health, T.H. Chan School of Public Health, Harvard University, 655 Huntington Ave Boston, MA 02115, USA

[c]Center for Excellence in Regional Atmospheric Environment, Institute of Urban Environment, Chinese Academy of Sciences, Xiamen 361021, China

[d]School of Materials Science and Engineering, Nanyang Technological University, 50 Nanyang Avenue, Singapore 639798, Singapore

[e]Environmental Chemistry and Materials Centre, Nanyang Environment and Water Research Institution, 1 Cleantech Loop, CleanTech One, Singapore 637141, Singapore

[f]School of Biological Sciences, Nanyang Technological University, 637551, Singapore

[#] These authors contributed equally to this work.

Abstract

The potential genotoxic effects of engineered nanomaterials (ENMs) may occur through induction of DNA damage or disruption of DNA repair processes. Inefficient DNA repair may lead to accumulation of DNA lesions and has been linked to various diseases, including cancer. Most studies so far have focused on understanding the nano-genotoxicity of ENM-induced damages on DNA while the effects on DNA repair have been widely overlooked. The recently developed fluorescence multiplex host cell reactivation (FM-HCR) assay allows for the direct quantification of multiple DNA repair pathways in living cells and offers a great opportunity to address this methodological gap. Herein, a FM-HCR-based method is developed to screen the impact of ENMs on six major DNA repair pathways using suspended or adherent cells. The sensitivity and efficiency of this DNA repair screening method was demonstrated in case studies using primary human small airway epithelial cells and TK6 cells exposed to various model ENMs (CuO, ZnO, and Ga_2O_3) at sub-cytotoxic doses. It was shown that ENMs may inhibit nucleotide excision repair, base excision repair, and repair of oxidative damage by DNA glycosylases in TK6 cells, even in the absence of significant genomic DNA damage. Of note, DNA repair capacity was increased by some ENMs while suppressed by others. Overall, this method can be part of a multi-

[¥]To whom correspondence should be addressed: Prof. Philip Demokritou, pdemokri@hsph.harvard.edu, Tel.: +1 617-432-3481, co-corresponding author: Dr. Zachary D Nagel, znagel@hsph.harvard.edu.

Conflicts of interest

The authors declare no conflict of interest

Author Manuscript Author Manuscript Author Manuscript Author Manuscript

tier, *in vitro* hazard assessment of ENMs as a functional, high-throughput platform that provides insights to the interplay of properties of ENMs, DNA repair efficiency, and genomic stability.

Graphical Abstract

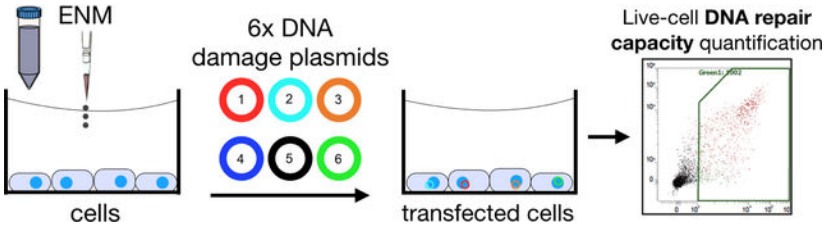

Keywords

DNA repair; DNA damage; engineered nanomaterials; genotoxicity; FM-HCR

Advances in the field of nanotechnology have enabled the synthesis of engineered nanomaterials (ENMs) that have led to the development of commercial products and applications in the health,[1] food,[2,3] and agriculture,[4–7] energy,[8] electronics, and construction industries,[9,10] among others. For example, superparamagnetic iron oxide ENMS have been used *in vivo* for the targeted delivery of docetaxel to solid tumors *in vivo*,[11] biopolymer-based ENMs are considered for use in the food and pharmaceutical industry,[12–16] carbon nanotubes have improved the mechanical properties of materials in the construction industry,[17] and graphene has enabled experiments that have advanced our understanding of quantum phenomena.[18] Continuous investment in nanotechnology will lead to more applications for ENMs[19] and further increase human exposure in occupational settings,[20–23] at the end-consumer level,[24] and during the lifecycle of nano-enabled products.[25,26] Under these circumstances, ENMs are under scrutiny in order to clarify the risks they pose for human health and to ensure the safe and sustainable use of nanotechnology.[27–31]

A growing body of literature suggests that due to their high reactivity, enormous surface area, chemical composition, and ability to interfere with biological structures, ENMs may exert cytotoxic and genotoxic effects on various biological sytems.[32–36] Their adverse effects have been attributed to direct damage on physiological barriers,[37] deleterious effects on organelles including mitochondria and lysosomes,[38,39] and the induction of intracellular and extracellular reactive oxygen species (ROS).[40–43] ROS may lead to persistent inflammatory responses and genotoxicity,[44] conditions that have been strongly correlated with serious diseases, including pulmonary fibrosis and cancer.[45]

DNA is the most important biomolecule as it stores genetic information in mammalian cells, and is vulnerable to DNA damaging agents, including ionizing radiation[46,47] and chemicals.[48] Many cancers are attributable to environmental DNA damaging agents,[49] and several studies have observed DNA damage upon exposure to ENMs, mainly due to excess generation of ROS.[50] Indeed, excess ROS following exposure of cells to ENM induces oxidative base damage, apurinic/apyrimidinic sites, single-strand breaks (SSBs), double-strand breaks (DSBs)[51,52] and epigenetic effects.[53,54]

Author Manuscript Author Manuscript Author Manuscript Author Manuscript

DNA repair pathways continuously detect and remove DNA lesions. Unrepaired DNA lesions can lead to cell death or cancerogenic mutations.[55] The sum of DNA repair processes is crucial for maintaining cellular health and is intertwined with other cellular responses, such as intracellular signaling, apoptosis, telomere maintenance, replication, cell division, cell cycle checkpoints, senescence, immune activation, metabolic changes, and inflammation.[56,57] In order to maintain genome stability, there exist several DNA repair pathways each of which specializes in repairing different types of DNA lesions. Base damage and abasic sites are predominantly repaired by the base excision repair (**BER**) pathway. The first step involves recognition and removal of damaged bases by DNA glycosylases. For instance, repair of alkylated bases is initiated by methylpurine-DNA glycosylase (**MPG**), repair of 8-oxoguanine opposite cytosine (**8oxoG:C**) is initiated by 8-oxoguanine DNA glycosylase (OGG1) and Nei-like DNA glycosylases (NEIL1, and NEIL2), whereas removal of an undamaged adenine base opposite 8oxoG (**A:8oxoG**) is initiated by the mutY DNA glycosylase (MUTYH).[58–61] DNA glycosylases leave behind an abasic site that is then processed by apurinic or apyrimidinic endonuclease (APE1). APE1 incises the abasic site to produce a SSBs, which is then processed by one of two sub-pathways of BER (short or long patch) depending on the precise chemistry of the DNA ends and the availability of BER enzymes. Bulky DNA adducts that distort DNA and block DNA replication are repaired by the nucleotide excision repair (**NER**) pathway.[62] Most DSBs are either repaired by non-homologous end joining (**NHEJ**) or homologous recombination (HR) depending in part on the precise chemistry of the DNA ends and the stage of the cell cycle.[63]

Exposure to chemicals and others stressors that interfere with the efficiency of DNA repair processes can lead to genomic instability.[52] This potential mechanism of genotoxicity is distinct from direct induction of DNA damage and could pose a health risk to exposed populations. Indeed, deficiencies in DNA repair capacity (DRC) are associated with increased cancer risk, immune dysfunction, and neurocognitive disorders,[64–66] and modest deficiencies on the order of 10–20% are associated with many types of cancer.[58,67] Table 1 presents examples of non-congenital disorders and non-hereditary diseases possibly associated with imbalanced DNA repair capacity relevant to the pathways studied here.

Genotoxic effects of particulate stressors on DRC are challenging to quantify due to limitations imposed by available techniques and, as a result, they have been understudied in the nanosafety field. Firstly, population studies of particles' genotoxic effects, *e.g.*, upon occupational exposure, are subject to several confounding environmental stressors which also alter DRC, like UVA and UVB radiation.[68] Secondly, most of the *in vitro* assays employ DNA damage/repair kinetics[69] (*e.g.*, comet assay or γ-H2AX staining), identification of chromosomal aberrations (*e.g.*, cytokinesis blocked micronuclei formation), transcriptional profiling (*e.g.*, real time PCR, RNA seq, microarrays),[51,70–76] proteomics studies,[77–80] acellular assays (fluorescence hybridization assay), measurement of DNA repair enzymatic activity (using cell lysate for BER, MMR or different lesions), and high-performance liquid chromatography/electrochemical detection require cell lysate or the cells to be in a different homeostatic condition - both parameters that may induce genotoxic stress and artificially sensitize the cells' DNA repair systems. Also, some of the aforementioned assays suffer from low sensitivity, may rely on indirect measurements, or have low statistical

Author Manuscript Author Manuscript Author Manuscript Author Manuscript

power. Importantly, most of these methods struggle to capture changes occurring in homeostatic environments following exposure of cells to ENMs due to epigenetic or post-translational regulations and rather focus on a single DNA repair pathway. Consequently, it is not possible to understand the inter-connected role of multiple DNA repair pathways upon exposure to huge libraries of ENMs or correlate specific particle traits to genotoxic responses.

Here, this methodological gap was addressed with a streamlined platform for assessing DRC upon exposure to ENMs. This platform makes use of emerging, fluorescence-based multiplex host cell reactivation (FM-HCR) assay previously described by Nagel *et al.*[81] for chemicals and ionizing radiation. This functional assay enables the direct assessment of multiple DNA repair systems upon exposure to ENMs. FM-HCR reports the ability of living cells to repair damaged reporter plasmid genes. The methodology takes advantage of the exquisite sensitivity of RNA polymerase to the presence of DNA lesions, which disrupt transcription and thus the expression of fluorescent reporter proteins, as described elsewhere.[82,83] Reporter plasmids with chemically defined site-specific DNA lesions are transiently transfected to adherent or suspended cells and provide live-cell readouts for all major DNA repair pathways or enzymes involved in repairing DNA lesions following exposure to ENMs. Ultimately, this high-throughput and sensitive platform was used to assess the effects of ENMs on the DRC of both adherent and cells in suspension.

Results and discussion

Figure 1 summarizes the developed method for quantifying DNA repair capacity (DRC) of living cells exposed to ENMs. Firstly, well-characterized ENM powders are dispersed in cell culture medium (Figure 1A) and administered to either adherent cells or cells in suspension (Figure 1B). The dosimetric analysis of ENM is highly recommended because it enables dose-matched, inter-particle comparisons of biological effects on adherent cells.[84] To quantify DRC, six types of reporter plasmids carrying equal number of DNA lesions are first engineered (Figure 1C - **Step I**) and then transfected to cells previously exposed to ENMs (Figure 1C - **Step II**). Cells in suspension are optimally transfected through electroporation, whereas adherent cells are transfected with the use of lipofectamine. Twenty-four (24) hours post transfection, DRC for all six lesions is quantified by means of flow cytometry based on the ability of cells to repair the reporter plasmids and restore their fluorescence (Figure 1C - **Step III**). The aforementioned steps are both ENM- and cell-specific and required fine-tuning. The development and optimization of this integrated method is presented in detail in the method section.

Characterization of ENM powders.

Table 2 summarizes the results of the primary particle characterization of gallium oxide (Ga_2O_3), copper oxide (CuO), and zinc oxide (ZnO) ENMs. In brief, SSA values for ZnO, CuO, and Ga_2O_3 ENMs were 16 g/m^2, 14 g/m^2, and 251 g/m^2, respectively. All particles had a near spherical shape and homogeneous morphology, as observed by transmission electron microscopy (TEM) (Figure S1 A and B) and their mean particle diameters were 46 nm and 50 nm for ZnO and CuO ENMs, respectively. The very small size, fractal geometry,

Author Manuscript Author Manuscript Author Manuscript Author Manuscript

and sintered necks of Ga_2O_3 did not allow for size measurements using TEM, although the primary particle size was clearly below 5 nm (Figure S1 C). Details on physicochemical characterization data for ZnO and CuO ENMs have been presented by the authors in previous publications.[31] Finally, microbiological evaluation of all ENM powders was negative (0 bacteria/mg) and endotoxin levels were below 5 EU/mg.

ENM dispersion, colloidal characterization, and dosimetric analysis.

As summarized in Figure 1A, the dispersion preparation of CuO, Ga_2O_3, and ZnO ENMs was performed according to a protocol previously developed by the authors[85] (see Materials and methods for more details). The critical delivered sonication energy (DES_{cr}) is defined as the minimum acoustic energy per suspension volume required to disperse ENMs in deionized water (DI H_2O) at the smallest possible agglomerate size.[86] DSE_{cr} was 76, 416, and 420 J/mL for Ga_2O_3, CuO, and ZnO ENMs, respectively. Table 3 presents the colloidal properties of ENMs in water and in cell culture media, once particles were sonicated at DSE_{cr}. These include hydrodynamic diameters (d_H), polydispersity index (PDI), zeta-potential (ζ), and effective density. In DI H_2O, all ENMs used in this study formed suspensions with small PDI values (0.19 – 0.33), an indication of relatively uniformly sized agglomerates. d_H for CuO and ZnO ENMs in DI H_2O were ~0.4 and ~0.3 μm, respectively, suggesting few-particle clustering. Ga_2O_3 ENM appeared to create multiple-particle clusters with average d_H ~0.1 μm. All ENM suspensions in water presented modest to strong ζ-potential values ($|\zeta|$ ranged from 14 to 38 mV). In cell culture media, ENMs showed variable degrees of culture medium-dependent agglomeration. ZnO and CuO ENMs only agglomerated in fully supplemented RPMI, while they did not present strong agglomeration in small airway epithelial cell growth medium (SAGM). Figure S2 A–C presents the intensity-weighted d_H distributions of all three ENMs in DI H_2O and fully supplemented RPMI and SAGM.

When possible, it is important that inter-particle toxicological comparisons take into consideration the variable particokinetics of ENMs *in vitro*.[85] This allows comparisons of ENMs on the basis of metrics like ENM mass delivered to cell surface area. An integrated approach for the dispersion preparation, colloidal characterization, and dosimetric analysis of ENM in cell culture media for adherent cell lines[87] was recently developed by the authors and applied here for ENMs suspended in SAGM. Following their dispersion, the effective density (ρ_{eff}) of ZnO, CuO, and Ga_2O_3 ENMs was calculated using the Harvard volumetric centrifugation method[88] and found to be 1.13, 6.15, and 6.16 g/mL, respectively. Based on the volume-weighted d_H (as measured by DLS) and their ρ_{eff}, their normalized delivered-to-cell mass fraction as a function of time (f_D), was calculated and presented in Figure S2 D. Due to smaller agglomerate size and primary particle density, ZnO ENM deposited at slower rates on cells, while Ga_2O_3 and CuO ENMs had similar f_D under the experimental conditions of the study.

High-throughput screening of DNA repair capacity alterations by ENM based on FM-HCR.

The development of FM-HCR as a tool for nanosafety research required the use of sub-cytotoxic doses of ENM, optimization of transfection efficiency, and adjustment of several flow-cytometry parameters. Appropriate controls with untreated cells and strong adherence

Author Manuscript Author Manuscript Author Manuscript Author Manuscript

to good laboratory practices for molecular biology should be followed to minimize to the extent of possible errors that could be introduced during transfection due to handling of cells and biological reagents. Such optimizations are ENM- and cell-specific. Results from the development process described in method section are presented below:

Cell Exposure to ENM to define dose-cytotoxicity relationship: Given the objective to measure DRC in *living* cell populations, it was crucial to expose cells at sub-cytotoxic levels of ENMs. SAEC and TK6 cells were exposed to ENMs following their dispersion in their respective cell culture medium at various concentrations for 4 or 24 hours, as shown in Figure 1B (see Materials and methods for details). The 4- and 24-hour time-points were chosen based on the ENM particokinetics and the biology of the cells. First, the deposited-to-cell ENM mass fractions are contingent on their respective particokinetics, as shown in Figure S2D. Second, DNA damage-induced stress responses peak between 4 and 24 hours.[89] While 4-hour time-points should capture early events, 24 hours provide sufficient time for most cell lines to undergo a population doubling and thus ensures that ENM interact with cells through all phases of the cell cycle, possibly revealing variable sensitivities to ENMs.[90] Figure S3–A shows that at 4 hours, the highest, non-cytotoxic dose delivered to SAEC was 15.6 μg/cm^2 for all three ZnO, CuO, and Ga_2O_3 ENMs, as measured by extracellular release of LDH. At 24 hours, all model ENMs showed ~10% cell death at an even lower dose delivered to cells (1.6 μg/cm^2). It is worth noting that the doses delivered to adherent cells were matched following the dosimetric methodology described above by adjusting their administered dose.

Additionally, Figure S4–A shows that at 4 hours, the highest, non-cytotoxic dose for TK6 cells was 100 μg/mL for ZnO and Ga_2O_3 ENMs and 10 μg/mL for CuO ENMs. At 24 hours, the non-cytotoxic dose of ZnO and Ga_2O_3 ENMs dropped to 10 μg/mL, whereas CuO ENM could decrease the viability of TK cells at even 1 μg/ml. Complete toxicological screening, including quantification of intracellular reactive oxygen species and metabolic activity, are also presented in Figures S3 and S4 for SAEC and TK6 cells, respectively. It has to be noted that the assessment of cytotoxicity is necessary to ensure that only non-cytotoxic ENM doses are used when performing the FM-HCR assay. Other effects, like ROS generation and mitochondrial metabolic activity, may not be correlated with potential changes in DRC as these are independent phenomena that are measured at the time of transfection, with DRC reflecting the ability of treated cells to repair DNA damage over the subsequent 24 hours.

TK6 cells (human lymphoblast) were used in this study as a cell model due to their high proliferation rate and stable karyotype which allow for comprehensive genotoxicity analyses in a human-relevant test system which makes them an ideal test line for chemicals and ionizing radiation.[91] SAEC were isolated from the distal portion of human respiratory tract and were used in this study as a representative type of normal human tissues likely to be exposed to inhalable ENMs. In fact, SAEC have been extensively used for studies of pulmonary-related inflammation or changes of the small-airway epithelium following exposure to various types of exogenous stressors.[43,92,93] It is important to note that SAEC were exposed to ENM on the basis of delivered particle mass per cell surface area. The dosimetric analysis based on ENM particokinetics in SAGM allowed to match the delivered particle dose after 4 or 24 hours for all three ZnO, CuO, and Ga_2O_3 ENMs. On the contrary,

Author Manuscript Author Manuscript Author Manuscript Author Manuscript

TK6 cells grow in suspension and inter-particle comparisons were performed based on administered ENM concentration (μg/mL).

Optimizing efficiency of reporter plasmid transfection.—Figure 1C - **Step I** represents the engineering of plasmids carrying DNA lesions repairable by distinct DNA repair mechanisms. Six different reporter plasmids each bearing different DNA lesions were transiently transfected into cells to assess the repair capacity in multiple DNA repair pathways as summarized in Table 4. The NHEJ pathway was measured using a reporter plasmid with an enzymatically generated DSB; long patch BER was measured using a plasmid bearing a site-specific tetrahydrofuran abasic sites analog; NER was measured using a reporter plasmid that was subjected to UV irradiation. For these three reporters, the DNA lesion blocks transcription and thus prevents fluorescent protein expression unless repair occurs by the indicated pathway. Accordingly, DRC is directly proportional to expression of these reporter plasmids. Initiation of BER by methylpurine DNA glycosylase (MPG) was measured using a reporter plasmid with a site-specific hypoxanthine (Hx) adduct. Initiation of BER of oxidative damage, which is catalyzed by several DNA glycosylases including OGG1, NEIL1 and NEIL2, was measured using a reporter plasmid with a site-specific 8oxoG lesion in the transcribed strand. Initiation of BER by MUTYH, which removes adenine opposite 8oxoG was measured using a reporter plasmid with an undamaged adenine in the transcribed strand opposite 8oxoG. For these three reporters, the DNA lesion alters the sequence of the transcribed RNA in a manner that leads to expression of a fluorescent protein.

Accordingly, DNA repair capacity is inversely proportional to expression of these reporter plasmids, and we have reported repair capacity as the reciprocal of fluorescent reporter expression. In the case of complete repair, these assays yield 0% reporter expression, and the reciprocal is undefined. In these situations, or where quality control metrics were not met, no data were plotted (see "*Optimization of reporter plasmid transfection efficiency*").

Before the transfection of SAEC or TK6 cells with the engineered plasmids, it is important to replace the ENM-containing medium with fresh medium. This is necessary to minimize the accidental introduction of potentially fluorescent ENM in the cells during transfection which could have unpredictable genotoxic effects or lead to the recording of false positive events. Moreover, it circumvents possible interactions of ENM with plasmid DNA, which have been heavily reported, especially for positively charged ENM.[94] The plasmids were then transfected to either SAEC or TK6 cells, as represented in Figure 1C - **Step II**. Here, it has to be noted that there is a fixed time window of ~24 hours between the transfection and the fluorescence-based quantification of the reporter plasmid expression by flow cytometry. During this time-window, some short-term transcriptional events related to DNA repair capacity may be missed. For quality control purposes, 10 fluorescent cells and transfection efficiency above 0.1% were set as a minimum threshold for data inclusion. These criteria were also met for SAECs with the use of lipofectamine for FM-HCR analysis, as shown in Figure S5. More details on the parametrization of SAEC transfection through lipofectamine, including the required control measurements can also be found in Figure S5. Transfection of lymphoblastoid cell lines including TK6 has been optimized in our previous study[81] and more details can be found in the methods section.

Author Manuscript Author Manuscript Author Manuscript Author Manuscript

To expand the usability of FM-HCR technology in the nanosafety field and quantify alterations in DRC following exposure of cells to ENM, the method was optimized for adherent, primary human SAEC which are widely used for inhalation exposure studies. It is important to note that primary human cells, like SAEC, may not tolerate transfection as well as immortalized cell lines. Indeed, electroporation using MXCell 96-well plates (at 260V/950 μF) was highly toxic to SAECs, as shown in Figure S5A. Transfection using lipofectamine led to both higher levels of cell viability *and* transfection efficiency, as shown in Figures S5B and S5C. The internal transfection controls were pmax_mOrange for damaged cocktail 1, and pmax_BFP for damaged cocktail 2. Fluorescent reporter expression for each plasmid was normalized to the expression of the internal transfection control plasmid. After this normalization, the expression of each damaged reporter plasmid was normalized to its undamaged counterpart to calculate percent reporter expression. Finally, percent reporter expression for ENM treated cells was normalized to that for untreated controls. This final normalization makes the assay more robust to potential batch effects. When such effects from day-to-day variabilities do not need to be considered, it is also possible to directly compare the raw signals between reporter expression of untreated and ENM-treated cells. It is expected that the proposed transfection approach can be successfully applied on other adherent cells and cell lines, however plasmid transfection efficiency and cell viability should always be verified and optimized as performed in this study.

Fine-tuning flow-cytometry parameters for cells exposed to ENMs.—Figure S7 shows that ENM treatment resulted in a leftward shift of the main population of cells in the FSC *vs* SSC plot. However, no difference was observed in reporter expression (NHEJ, long patch BER, NER, Hx(MPG), 8oxoG:C, A:8oxoG) upon adjusting the gating conditions to accommodate the observed shift as shown in Figure S7A and S7B. Moreover, a single set of gates was used to analyze all samples so as to minimize variability, as presented in Figures S6A and S6B. Figure S8 presents example flow-cytometry data of cells transfected with and without ENMs for different reporter plasmid cocktails.

Fine-tuning the flow-cytometry parameters, including adjustment of gating, fluorescent voltages, and exclusion of doublets, was key in adapting FM-HCR to the field of nanosafety. For example, additive fluorescent events or false positives in the reporter gates could be generated by culture media alone or dispersed ENM, as indicated in Figure S6C. Indeed, ENMs tend to decrease their surface energy by means of physisorption of biomacromolecules, including proteins[95] and plasmid DNA,[96] and could thus alter the functionality of reporter plasmids. Furthermore, ENM scatter light and their intrinsic fluorescence may generate signals detectable by flow cytometry, even in complex biological media.[97,98] Finally, cell morphology may change upon exposure to ENM[99] which may in turn alter their scattering properties, as observed here for TK6 cells. Adjustment of flow-cytometry parameters in response to these phenomena carries the risk of excluding a subset of cells or introducing variability. Therefore, these quality control steps are essential to ensure that all transfected cells are accounted for in the obtained data and that all obtained data are only due to the transfected cells. More information on the exact parameters employed for flow-cytometry can be found in the methods section.

Author Manuscript Author Manuscript Author Manuscript Author Manuscript

Case studies: assessing nanoparticle-mediated alterations in DNA repair capacity using the FM-HCR methodology.

The developed method was applied on TK6 cells exposed to ZnO, CuO, and Ga_2O_3 ENMs as case studies that demonstrate its ability to resolve variable particle effects on genomic stability. This specific panel of ENMs was put together because they have already found their way in commercial products and industrial processes and thus pose a possible risk for human exposure.[100] The method was applied following 4- and 24-hour ENM exposures to inquire its sensitivity in detecting early changes in DRC. Under select conditions, the method was also applied on SAEC to demonstrate its applicability on adherent, human primary cells. Results on a case-by-case basis are elaborated below.

ZnO ENM: Upon exposure of TK6 cells to ZnO ENM at 100 μg/mL for 4 hours, some DNA repair pathways were induced while others were inhibited. Specifically, significant decreases were observed in long patch BER ($p=0.02$) and NER ($p=0.01$) reporter expression, while accompanied by a significant increase ($p=0.02$) in repair for Hx(MPG), as shown in Figure 2A and 2B. Moreover, at 10 μg/mL over 24 h, there was a significant and considerable (by ~10%) decrease in A:8oxoG lesion repair, as shown in Figure 2B. Already, FM-HCR reveals that exposure to ENMs may simultaneously and differentially affect multiple DNA repair pathways in a dose- and exposure duration-dependent manner. It is important to note here that mitochondrial activity and released LDH did not indicate acute cytotoxicity under the aforementioned conditions, although there was a doubling in production of intracellular ROS after 4h at 100 μg/mL. In accordance to the literature[101] and our own previous work,[69] significant increase in oxidative damage and strand breaks in TK6 cells exposed to ZnO ENMs, as presented in Figure 2D was demonstrated. Specifically, a significant and considerable increase (+40%, 95%CI: −42.51 to −31.36, $p<0.0001$) in DNA damage was induced at 100 μg/mL over 4h, but this effect was not present at lower concentrations. These data highlight the complementary information provided by the two types of assays. Comet assays provide a snapshot of DNA damage levels, whereas the FM-HCR assays provide a measure of DNA repair, both important metrics for genotoxicity studies. Importantly, alkaline comet assays detect strand breaks and DNA lesions, such as abasic sites, that can be converted into SSBs under alkaline conditions. Since the NER pathway primarily repairs bulky DNA adducts, unrepaired DNA damage associated with ENM-induced NER inhibition would not be detected by conventional comet assays.

The complex effect of ZnO ENM on DRC of TK6 cells led us to expose SAEC at delivered to cell dose of 1.6 μg/cm^2 for 4 hours which were non-cytotoxic as shown in Figure S3. Under these conditions, a significant ($p=0.009$) difference in A:8oxoG reporter expression was observed, as shown in Figure 2C. At this delivered to cell dose, no DNA damage was detected by the alkaline nano-CometChip assay. In fact, Figure 2D shows that DNA damage only increased in a considerable and significant manner (95%CI: −61.65 to −43.29, $p<0.0001$), when SAEC were exposed to 15.6 μg/cm^2 for 4 hours. This highlights the ability of FM-HCR assays to detect alterations in DNA repair at doses that do not result in DNA damage detectable by comet assays. The magnitude of the detected changes in DRC are large enough to be of concern for cancer risk, particularly under conditions of sustained exposure.

Author Manuscript Author Manuscript Author Manuscript Author Manuscript

A central question concerns the establishment of a threshold for changes in DRC in ENM-exposed cells that can be used to flag the material for follow-up with further genotoxicity assessments. The answer depends on whether DNA damage that would normally be repaired by the disrupted pathway is present in the exposed tissue. This DNA damage can arise endogenously, or it may be induced by environmental agents, including in some cases the ENMs themselves. For example, simultaneous skin exposure to sunlight and an ENM that inhibits NER may increase risk of UV-induced skin cancers. In general, inhibiting DNA repair can lower the threshold for genotoxicity due to a second exposure.[102]

We propose a 50% change in DRC in exposed cells as a conservative threshold for follow-up with additional assays testing for genotoxicity of previously uncharacterized ENMs, provided the change in repair capacity is dose-dependent and occurs at physiologically relevant doses. We base this threshold on numerous epidemiological studies using functional assays have demonstrated that differences in repair capacity on the order of 10–20% are associated with increased cancer risk, with odds ratios of 2 or more.[58] Notably, an increase in repair capacity can also be a risk factor; higher levels of MPG activity, which we observed in ZnO ENM-treated TK6 (see Figure 2B), are associated with increased lung cancer risk.[103] This counter-intuitive excess cancer risk in individuals with elevated DRC may be attributable to a phenomenon referred to as repair imbalance, wherein an early step in the repair process (in this case, MPG-catalyzed initiation of base excision repair) leads to the accumulation of downstream repair intermediates that may be more cytotoxic and mutagenic than the initial base lesion.[104] As has similarly been proposed for other genotoxicity assays such as the Ames test,[105] follow-up with mutation assays can determine whether an ENM increases the mutagenicity of agents that produce DNA damage normally processed by the pathway flagged by our FM-HCR platform.

Our findings that ZnO ENM leads to less efficient BER and elevated levels of DNA damage are broadly consistent with previous studies. For example, it has been shown that exposure to ZnO nanoparticles (50–80 nm in diameter) promoted the formation of micronuclei in TK6 cells and led to slower DNA repair kinetics in human SHSY5Y neuronal cells.[106,107] Similarly, Zinjo *et al.* observed induction of micronuclei, DNA strand breaks, Fpg sensitive sites, and slower removal of 8oxoG lesions from the genome in Caco-2 cells following exposure to ZnO nanoparticles.[108] Finally, the same type of particles reduced the viability of murine macrophages by leading to G0/G1 cell cycle arrest, inhibited the action of superoxide dismutase, and decreased the activity of long patch BER enzymes PolB and FEN1.[78] Decreased PolB and FEN1 activity would be consistent with our observation of diminished long patch BER activity in TK6 cells upon exposure to ZnO ENM. Consistent with our observation of diminished NER activity in TK6 cells treated with ZnO ENM, metal cations leached from ENM ($CdSO_4$, CdTe quantum dots, and ZnS) significantly reduce NER activity.[72,73,109] Specifically, the presence of Cd^{2+} in the nuclei of liver cells of zebrafish led to the formation of bulky DNA adducts formation after an exposure of zebrafish to CdTe quantum dots.[73] ZnO ENMs are also prone to intracellular dissolution, and therefore increased nuclear concentration of Zn^{2+} is a possible mechanism underlying the observed alterations in DNA repair pathways. Our data suggest that ENM dose and exposure duration may affect multiple cellular processes in a non-linear and non-monotonic relationship. For example, NER activity is increased at 10μg/mL of ZnO ENM but inhibited at 100μg/mL.

Author Manuscript Author Manuscript Author Manuscript Author Manuscript

One potential interpretation is that ZnO ENMs induce an adaptive and protective DNA damage response at low doses similar to that induced by ionizing radiation and other agents.[110] Above a certain threshold, this response may be offset by metal-dependent inhibition of NER, which has been previously reported for Cd(II) and As(III).[81]

CuO: Figures 3A and 3B show that upon exposure of TK6 cells to CuO ENM at 10 μg/mL for 4 hours, there was a significant ~30% decrease in long patch BER (p=0.01) and MUTYH-dependent excision of A:8oxoG (p=0.05). In addition, there was evidence of an increase in repair activity for 8oxoG:C lesions, signified as "N/A" (Figure 3B). Note that for this assay, repair capacity is inversely proportional to reporter expression; for this reason, the absence of detectable signal reflects higher repair capacity. Importantly, exposure to of TK6 to 10 μg/mL h of CuO ENM over 4 h did not induce considerable DNA damage as measured by comet assays compared to the untreated control (+2%, 95%CI: −1.628 to −0.5734, p=0.0003), as shown in Figure 3C. Despite the absence of considerable DNA damage, intracellular ROS levels appeared very elevated compared to the untreated control (+70%, Figure S4e). The higher toxicity of CuO ENMs at 10 μg/mL compared to 100 μg/mL could be attributed to increased particle agglomeration at higher concentrations which decreases the available agglomerate surface area and may inhibit the release of Cu^{2+}, both of which are important mediators of nanoparticle toxicity.[111,112] The apparent discrepancy between elevated ROS levels and minimal DNA damage might be due to accentuated repair of oxidative damages, as reported by the FM-HCR assays (Fig 3B). Here, it is worth mentioning that DNA repair pathways were differentially affected in TK6 cells following exposure to CuO ENM than they did to ZnO ENM, attesting to the ability of FM-HCR to resolve ENM-specific biological responses. Application of the FM-HCR assay at higher particle doses (*e.g.*, 100 μg/mL) or over longer exposure times (*e.g.*, 24 hours) was not possible due to the pronounced cytotoxicity of CuO ENMs. More information on the toxicological assessment of CuO ENM are presented in Figure S4a–d. Contrasts in DRC or toxicity observed among cell lines at higher *versus* lower doses of ENM exposure may reflect a non-monotonic dose-response, which has been observed for other agents such as bisphenol A.[113] Further detailed studies are needed for the test ENMs and doses used in this study to understand the potential underlying, ENM-specific biological mechanisms for DNA repair.

In our findings, CuO ENMs induce DNA damage and lead to an increase in DRC. These observations are consistent with previous characterizations of the effects of CuO ENM on cell lines. In more detail, oxidative stress, DNA damage, and a p53-dependent DNA damage response have been observed in A549 cells exposed to CuO nanoparticles.[77] p53 regulates several DNA repair pathways, including NER and BER.[114] In particular, p53 promotes the activity of glycosylases responsible for repair of oxidative damage,[115,116] consistent with the apparent increase in glycosylase initiated repair detected for FM-HCR substrates with 8oxoG:C and A:8oxoG lesions (Fig 3B). Furthermore, p53 negatively regulates APE1[117] -an enzyme responsible for initiation of repair of our long patch BER reporter- which is repaired less efficiently in CuO ENM exposed cells (Fig 3A). Further evidence for a CuO ENM-induced oxidative stress response came from a report by Semisch *et al.*, which demonstrated that A549 cells exposed to CuO ENMs undergo DNA damage-induced apoptosis.[118] Taken

Author Manuscript Author Manuscript Author Manuscript Author Manuscript

together, the available data indicate that our platform is capable of detecting alterations in DRC that occur as part of a p53-mediated DNA damage response that is mounted in cells exposed to genotoxic ENMs.

Ga_2O_3: Exposure of TK6 cells to Ga_2O_3 ENM at 10 μg/mL for 4h led to a significant increase (p=0.03) in NER reporter expression, as shown in Figure 4A. Interestingly, the cells' response was reversed after Ga_2O_3 ENM exposure at 100 μg/mL for 4h, with a return to baseline levels of, NHEJ, long patch BER, and NER reporter expression (Figure 4A and 4B). At the same time, Hx(MPG) and A:8oxoG repair pathways presented an increasing, albeit statistically insignificant trend. In accordance to other studies, our cytotoxic and genotoxic assessment of Ga_2O_3 ENM was negative, bolstering their innocuous toxicological profile. Supporting comet assay and toxicological assessment are presented in Figure 4D and in Figure S3 a–e, respectively. While inhibition in DNA repair may have well-known adverse effects, induction of these pathways can also be an indicator of genotoxicity. Induction of DNA repair pathways can be indicative of a DNA damage response, and as mentioned above can have deleterious effects due to an imbalance of multi-step repair processes.

Regarding the mechanism underlying the observed effects, it has to be noted that Ga_2O_3 ENMs are insoluble in aqueous media, therefore it is not expected that metal ions are the culprit of the observed biological responses. Although more studies are required to elucidate how Ga_2O_3 ENM impact DNA repair, enhanced particle internalization and nuclear localization have been observed for small ENMs,[119] pointing to the possibility of direct particle interference with the dynamic multi-protein machines that carry out DNA repair.

The important effects of Ga_2O_3 ENM on TK6 cells and their small, inhalable size led us to expose SAEC to them at 1.6 μg/cm^2 for 4 hours. Toxicological results presented in Figure S4A–E and FM-HCR results shown in Figure 4C show that both exposure conditions were non-cytotoxic (<10% LDH release, no ROS generation), did not induce considerable genotoxicity (<10% DNA in tail), nor any changes in reporter expression were observed. Figure 5 provides an overview of the statistically significant DRC in SAEC or TK6 cells upon treatment with ZnO, CuO, or Ga_2O_3 ENMs. The starkly different responses of SAEC and TK6 cells to the same ENMs merits further investigation and is a reminder that statements about the safety of ENMs should be accompanied by ample contextual information regarding the route of exposure and biological system under consideration.

Conclusions

In this study, the development and versatility of a high-throughput method for assessing DRC alterations in human cells exposed to ENMs was demonstrated. Given the scarcity of DNA repair studies following exposure of human cells to ENMs, the proposed FM-HCR method has been designed to offer multiple advantages over previously used techniques. Compared to other techniques, this method provides a functional assay for living cells that directly quantifies alterations in six major DRC pathways within a streamlined workflow. Moreover, it only requires small numbers of cells, reports the effects of ENMs under physiological conditions (instead of cell lysates) thus avoiding the use of detergents and

Author Manuscript Author Manuscript Author Manuscript Author Manuscript

other reagents that could alter the properties of ENMs. Finally, its low cost and semi-automated analysis removes subjective bias and democratizes the testing of crucial genome repair processes in ENM exposed cells.

Beyond its proven use with cells in suspension (*e.g.*, TK6), FM-HCR was adapted here for cells routinely used in nanosafety studies, like sensitive, adherent, primary human cells. The engineering of plasmids with site-specific DNA lesions also enabled functional analysis of the molecular mechanisms underlying 6 major DNA repair pathways in cells exposed to multiple types of ENMs. Importantly, FM-HCR assays integrate the contributions of a complex series of steps that may be impacted by exposure to ENMs into a simple functional readout. We have integrated critical controls into the workflow to eliminate potential interference from ENMs. These checkpoints do increase the required time to perform the assay, potentially rendering it more time-consuming than other techniques. Nevertheless, these optimization steps need only be performed once with each cell type-ENM combination. FM-HCR overcomes multiple challenges that limited the applicability of previous approaches and is thus a powerful tool for high-throughput screening of ENMs for predictive nanotoxicology and nanosafety.

While the scope of this methodological article study is focused on demonstrating the utility of FM-HCR platform in nanosafety research, we have also applied the developed methodology on a pilot scale to test whether disruption of DRC is an important mechanism by which ENMs can be genotoxic. The utility of FM-HCR as a sensitive screening tool for nanosafety research was demonstrated by the differential impact of ENMs to the studied DNA repair mechanisms. In particular, the extent of DRC alterations was found to be contingent on dose, exposure time, cell line, and ENM type. For example, ZnO ENM only increased the MPG DNA glycosylase activity in TK6 cells at the elevated dose of 100 μg/mL, while decreased excision of A:8oxoG at 24 hours of exposure at the much lower dose of 10 μg/mL. Another important finding was that exposure of cells to different ENMs may alter DRC in opposite directions. Specifically, exposure of TK6 cells to ZnO ENMs inhibited NER, while Ga_2O_3 ENM led to increased activity in the same pathway. The finding that some ENMs may induce higher DRC highlights the potential for adverse health effects of ENM exposure to be mediated not only by inhibition of DNA repair, but in some cases higher repair rates. Higher repair rates can lead to repair imbalance that promotes the accumulation of repair intermediates that can be more cytotoxic and mutagenic than the initial DNA lesions. Finally, SAEC exhibited different types of DRC alterations to TK6 following exposure to ZnO ENM, underscoring the important contributions due to cell type and route of exposure that must be taken into consideration when developing safe nano-enabled products and applications.

The biological effects of ENMs on cells and tissues *in vitro* are governed by a variety of factors that include the culture format (adherent or in suspension), dose, exposure time, endocytic mechanisms of ENMs, the exact composition of culture medium which defines their protein coronas,[120,121] and the fate of ENMs once inside the cell.[122] The biological effects of DNA damage also depend on a variety of factors including the ability of cells to process it, the severity and type of the damage, and the mechanisms by which it was induced. Taken together, these factors suggest that ENM genotoxicity may vary across cell

Author Manuscript Author Manuscript Author Manuscript Author Manuscript

types.[123] Therefore, it is important to perform genotoxicological screening using *in vitro* (and, later, *in vivo*) systems relevant to the exposed tissue. In this study, SAEC and TK6 cells are two vastly different types of cells, from the composition of their plasma membrane, to culture medium, and their potential to physically interact with suspended ENMs - all factors that play a role in ENM bioactivity.[124] It is also worth noting that the FM-HCR assay has been previously validated using a large number of cell types[81] and it is thus expected that the reported differences in the responses of SAEC and TK6 cells reflect the real differential biological differences between the two cell lines.

The FM-HCR method for ENMs demonstrated here complements more conventional toxicological assays and provide further insight to the effects of ENM on human cells. Of note, most effects detected and quantified by FM-HCR, like substantial inhibition in NER by ZnO ENM and significant increases in the activity of BER glycosylases by CuO ENMs, were not accompanied by acute cytotoxicity. Even more so, most of ENMs did not show DNA damage detectable by comet assays, but potentially genome-damaging effects of ENM were captured by FM-HCR. For example, NER inhibition by ZnO ENM was only evident by FM-HCR assay, suggesting that transient alterations in TK6 cells' DRC can be picked up by our platform. The finding that some ENMs may induce higher DRC highlights the potential for adverse health effects of ENM exposure to be mediated not only by inhibition of DNA repair, but in some cases higher repair rates. Higher repair rates can lead to repair imbalance that promotes the accumulation of repair intermediates that can be more cytotoxic and mutagenic than the initial DNA lesions.[125] Three of our FM-HCR assays report on the initiation step of BER, but unlike the assays for long patch BER, NER, and NHEJ, they do not report completion of repair. Notably, SAEC and TK6 exhibited different types of DRC alterations following exposure to ZnO ENM. This underscores the importance of taking the tissue type and potential routes of exposure into consideration when developing safe nano-enabled products and applications. As regards to the absolute magnitude of DRC alterations in either SAEC or TK6 cells as measured in the current study, these were generally small, even when statistically significant. Still, it has to be noted that errors in the genome that may accumulate due to exogenous factors (*e.g.*, radiation), or due to the inefficiency of endogenous DNA repair mechanisms like the ones studied here, may cause genomic instability. Such instability can lead to mutagenesis,[126] carcinogenesis,[62] and has also been linked to neurodegenerative diseases.[127] More recently, it was also suggested that, until repaired, DNA lesions may impact the cellular physiologic function to the same extent as genetic mutations.[128]

These case studies with FM-HCR assay are subject to some important limitations. FM-HCR is a powerful tool for measuring the activity of DNA repair pathways, but may not be sensitive to some chromatin structures that are only found in genomic DNA. Although comet assays complement FM-HCR in this regard, they are not sensitive to all types of DNA damage. Inhibition of DNA repair might not be sufficient to lead to mutations in the absence of a second insult. Therefore, studies using mutation assays to determine the joint effects of ENM exposure and exposure to a second DNA damaging agent, such as UV rays or ionizing radiation would be helpful for assessing mutagenicity in ENMs flagged by our platform as potentially genotoxic. Beyond the processes of DNA damage and repair, other key steps along the pathway to genotoxic effects would need to be considered to draw conclusions

Author Manuscript Author Manuscript Author Manuscript Author Manuscript

about the underlying mechanisms, and the likelihood that they will lead to adverse health outcomes in humans. These include identification of internalization pathways for each ENM, their sub-cellular localization, how they are processed in the physiological context of human tissues, and their dissolution inside cellular organelles, among others, but fall outside the scope of the current article.

As evidenced in this study, the development of FM-HCR enables the testing for potential genomic insults upon ENM exposure in the form of altered DRC. While DNA repair processes are understudied in the field of nanosafety, the assay's versatility in terms of studied cell types and diverse reporter plasmids with chemically defined DNA lesions should provide a high-throughput tool poised to improve the screening of ENMs. Results from its application suggest that DRC analysis could function as part of a tiered ENM screening to better inform more elaborate *in vivo* works or downstream proteomic analyses and thus help understand genotoxic adverse outcome pathways. The harmonization of methodological conditions through the development of assays like FM-HCR should allow for robust correlations between specific ENM properties, exposure settings, and promote the mechanistic understanding of possible pathogenic effects.[51,129]

Materials and methods

ENM synthesis.

In this study, a panel of 3 ENMs was used, namely ZnO, CuO, and Ga_2O_3. ZnO and CuO ENMs are reference engineered nanomaterials from the nanomaterials repository established at the Harvard University as part of the Nanotechnology Health Implications Research (NHIR) Consortium established by the National Institute of Environmental Health Sciences (NIEHS). ZnO and CuO ENMs were procured by Sigma Aldrich and Meliorum Technologies, Inc., respectively.

Ga_2O_3 ENM were synthesized in-house by the flame spray pyrolysis(FSP)-based Harvard VENGES system, according to a synthesis method described in detail elsewhere.[130–132] Chemicals for the synthesis of Ga_2O_3 ENM were purchased from Sigma-Aldrich and used without further processing.

ENM powder characterization.

TEM: Transmission electron microscopy (TEM, JEOL 2100) was used for primary particle size measurements and shape characterization of ZnO and CuO ENMs. To prepare the particles for TEM observations, 2 mg of each ENM powders were dispersed in DI H_2O at a final concentration of 0.5 mg/mL with the help of a cup-horn sonicator (please see the next section for more information on the dispersion protocol). The dispersion was then drop-cast on TEM grids (Ted Pella Inc., Redding, CA) and was left to dry for 10 min in an enclosed container. Blotting with filter paper was used to remove excess suspension. Images were obtained at 200 kV and were analyzed on ImageJ software (NIH). The Feret diameter was used to calculate the average primary particle diameter of the observed particles. Ga_2O_3 ENM were dispersed in ethanol prior TEM observation (Carl Zeiss Libra 120 Plus) at 120 kV. Image processing was performed as described for ZnO and CuO ENMs

Author Manuscript Author Manuscript Author Manuscript Author Manuscript

XRD: X-Ray diffraction (XRD) was used to define the crystal structure of ENM powders. The XRD patterns of ZnO and CuO ENMs were collected in 2θ at 10−90° configuration with a 0.02° increment and 2s step. Collected data were analyzed by EVA software by BRUKER©. For Ga_2O_3 ENM, XRD measurements were performed with a Rigaku Miniflex in a silicon low background holder and with a 1.25° divergence slit. The diffractograms were then analyzed in Rigaku's PDXL2 and Rietveld refinement performed where appropriate.

BET: N_2 adsorption was used to measure particle specific surface area (SSA, m^2/g) according to the Brunauer–Emmett–Teller (BET) theory. In brief, a 5-point BET isotherm was calculated using a surface area and pore size analyzer (Quantachrome Instruments, NOVAtouch LX4). Approximately 50 mg of ENM powder were degassed at 100–300 °C for >3 h. Average primary particle size (d_{BET}) was calculated assuming particle according to the following formula $d_{BET} = 6000/(SSA \cdot \rho)$, where, ρ is the material density in g/cm^3, and d_{BET} is in nm.

Microbiological sterility and endotoxin assessment: The biological sterility of ENMs was assessed according to the U.S. Pharmacopeia protocol for sterility (WHO document QAS/11.413) while their endotoxin load was quantified with the Recombinant Factor C (rFC) assay (Lonza PyroGene® kit) as suggested by manufacturer's instructions.

ENM dispersion, colloidal characterization, and dosimetric analysis.

Dispersion of CuO, Ga_2O_3, and ZnO ENMs in DI H_2O was performed according to a dispersion protocol previously developed by the autors.[86,88] In brief, ENM powders were added to DI H_2O at a final concentration of 0.5 mg/mL and underwent cycles of sonication (60 s) and high-speed vortexing (30 s) using a calibrated 3-inch cup-horn sonicator (Branson Sonifier S-450D, 400 W) and a bench-top vortexer, respectively. The cup-horn sonicator was calibrated according to a protocol previously presented elsewhere[88] and was found to deliver 1.23 W/ml. The sonication-vortexing cycles were repeated until there was no considerable change (± 5%) in their hydrodynamic diameter (d_H), as measured by dynamic light scattering (Zetasizer Nano ZS, Malvern UK) using 1 ml of the sonicated ENM suspension in optically clear cuvettes. At this point, the total acoustic energy delivered to the suspension (in J/mL) is termed critical delivered sonication energy (DSE_{cr}). The particles' ζ-potential values were measured upon delivery of DSE_{cr} using folded capillary cells. ENMs were then added in cell culture media (RPMI+ 10% vol/vol heat-inactivated FBS or SAGM) at a final concentration of 0.1 mg/mL where their colloidal properties (d_H, poly-dispersity index, ζ-potential) were also measured. Finally, the effective density (ρ_{eff}) of ENMs in SAGM was also measured according to the volumetric centrifugation method (VCM) described in our previous work[88].

The distorted grid (DG) model was applied to calculate the ENM concentration profiles along the wells of 96-well plates, the concentration at the bottom of the wells, and the fraction of administered ENM mass deposited onto the cell surface as a function of exposure time (f_D).[87,133] The particokinetics simulation was coded and executed on MATLAB (MathWorks, Massachusetts, USA).

Author Manuscript Author Manuscript Author Manuscript Author Manuscript

Cell culture

TK6 human lymphoblastoid cells from ATCC (American Type Culture Collection, USA) were used for the development and application of the methodology as a staple mammalian cell line for genotoxicity studies. TK6 cells were cultured in RPMI-1640 medium supplemented with L-glutamine, 10% vol/vol horse serum, and 100 U/mL streptomycin-penicillin in upright T75 flasks. TK6 cells were kept under humidified atmosphere of 37°C, 5% CO_2, and were used between passages 5 and 10. To demonstrate the applicability of the methodology on adherent cells, human primary small airway epithelial cells (SAEC) from Lonza Inc were used in the study. SAEC were maintained in basal medium mixed with required growth supplements (SAGM™ Small Airway Epithelial Cell Media BulletKit™), kept under humidified atmosphere of 37°C, 5% CO_2, and were used between passages 4 and 12.

Cellular treatment prior to fluorescence multiplex-host cell reactivation (FM-HCR) assay.

To expose TK6 cells prior to the FM-HCR assay, CuO, Ga_2O_3, and ZnO ENMs powders were dispersed in fully supplemented RPMI-1640 culture medium according to the procedure described above. Each of the CuO, Ga_2O_3, and ZnO ENM suspensions was then administered to log-phase growing TK6 cells in 24-well tissue culture plates at final ENM concentrations of 1, 10, and 100 μg/mL. The final volume of TK6 cell suspension was 0.8 mL and cell concentration was $2X10^6$ cells/ml. To expose SAEC prior to FM-HCR assay, cells were plated in 12-well plates and grown until 60–70% confluence at which point CuO, Ga_2O_3, and ZnO ENMs powders were dispersed in fully supplemented SAGM culture medium according to the procedure described above. Based on their particokinetics profile and f_D calculated as described above, each of the CuO, Ga_2O_3, and ZnO ENMs suspensions was administered to SAEC at starting concentrations that would lead to the deposition of 1.6 $\mu g/cm^2$ or 15.6 $\mu g/cm^2$, after 4 hours of exposure. Following ENM administration, SAEC and TK6 cells were kept under humidified atmosphere of 37°C, 5% CO_2 for the duration of the exposure (4h or 24h).

Cellular membrane integrity.

Following exposure to ENMs, the cellular membrane integrity of SAEC and TK6 cells was evaluated using the Pierce™ LDH Cytotoxicity Assay Kit (Thermo Scientific, Waltham, MA, USA). The released cytoplasmic enzyme lactate dehydrogenase was colorimetrically quantified in the supernatant of cells collected by centrifugation of suspended TK6 cells (300xg, 5 min) or by simple pipetting in the case of adherent SAEC. Briefly, 50 μl of the collected supernatant was transferred to a new 96-well plate, mixed with LDH assay reagent and incubated for 30min at room temperature protected from light. The absorbance values were recorded at 490 nm (LDH activity) and 680 nm (background signal from instrument) using a SpectraMax M5/M5e spectrophotometer (Molecular Devices, Sunnyvale, California). Maximum LDH release was measured in positive controls prepared upon treatment of cells with Lysis buffer 1X solution. LDH released for cells exposed to ENMs was compared to positive control and as percent LDH leakage (100×LDH release in medium of ENM-treated cells/maximum LDH release from positive controls) and expressed as the mean, using triplicate wells per concentration.

Author Manuscript Author Manuscript Author Manuscript Author Manuscript

Assessment of mitochondrial activity.

The reducing power of mitochondria and, in by extension, the viability of a cellular population can be estimated using the PrestoBlue® (Thermo Fisher, USA) assay. In brief, following 4h or 24h of ENM exposure, cell culture medium was removed by centrifugation of suspended TK6 cells (300xg, 5 min) or by simple aspiration in the case of adherent SAEC. Cells were washed with pre-warmed 1x PBS and the resazurin-based reagent was mixed with serum-free culture medium (10% vol/vol) and administered to cells before incubating them at 37°C from 30 min. Fluorescence signal from the reduced resorufin was detected using a SpectraMax M5/M5e with excitation at 560 nm and emission measured at 590 nm.

Measurement of intracellular reactive oxygen species.

CellROX® Reagent (orange) (Thermo Fisher, Waltham MA) was used to measure the intracellular levels of ROS following exposure of SAEC and TK6 cells to ENMs according to the manufacturer's instructions. Briefly, after exposure to ENMs, cell culture medium was removed after centrifugation of suspended TK6 cells (300xg, 5 min) or by simple aspiration in the case of adherent SAEC. Cells were then washed 3x with pre-warmed 1x PBS and CellROX® reagent was added at a final concentration of 5μM to the cells before incubating them for 30 minutes at 37°C in a CO_2 incubator. The reagent was then washed with pre-warmed 1x PBS as described above and cells were re-suspended in 1x PBS for fluorescence measurement with excitation at 480 nm and emission measured of 520 nm. As a positive control, cells were treated with 100 μM menadione for 1 hour at 37°C. Data were presented as relative increase of ROS levels compared to the untreated group.

Quantitation of DNA damage using alkaline single-cell nano-CometChip assay.

nano-CometChip (alkaline single-cell gel electrophoresis) was carried out to quantitate the amount of DNA damage induced by ENMs according to a protocol described by Watson *et al.*[69] In brief, 10,000 cells per 100μl/well were loaded for each cell type in 96-well plates (15 mins for TK6 cells and 30 mins for SAECs). After gravitational settling, excess cells were aspirated, and the chips were rinsed with 1X PBS. Then, molten low-melting agarose was overlaid onto the chip and allowed to set for 2 mins at 4°C. The chip was then submerged overnight at 4°C in ice-cold alkaline lysis solution (2.5 M NaCl, 100 mM Na_2EDTA, 10mM Tris, pH 9.5 with 0.5% Triton X-100). After overnight incubation, alkaline unwinding was performed using alkaline buffer (0.3M sodium hydroxide and 1mM Na_2EDTA in distilled water) at 4°C for 40 mins. Electrophoresis was carried out at 4°C for 30 mins at 21 V and 300mA and then the chips were neutralized using neutralization buffer (0.4 M Tris-HCl buffer, pH7.5). The chips were stained using 1X SYBR Gold nucleic acid gel staining (Invitrogen, Cat no # S11494) and fluorescent images of the comets were captured at 4X magnification using an epifluorescence microscope (Nikon Eclipse 80i, Nikon Instruments, Inc., Melville, NY) with a 480 nm excitation filter. Comet images were analyzed using Guicometanalyzer, a custom software developed in MATLAB (MathWorks Inc., Natick, MA). Outputs from Guicometanalyzer were processed and imported to Microsoft Excel using Comet2Excel, an in-house software developed in Python Software Foundation (Python

Author Manuscript Author Manuscript Author Manuscript Author Manuscript

version 2.7.10). The percentage of DNA in the comet tail was used as a parameter to measure DNA damage levels.

Assessing DNA repair capacity of cells using the FM-HCR assay.

Step 1: Preparation of reporter plasmids and cocktail composition for FM-HCR assay: Plasmid preparation was carried out as described in detail by Chaim *et al.*[82] and Nagel *et al.*[81] The selected DNA repair pathway/lesion studied were NHEJ-dependent repair of a restriction enzyme induced double strand break, NER-dependent repair of UV-induced DNA damage, long patch BER of a tetrahydrofuran abasic site analog, and repair of site-specific base lesions that report the activities of DNA glycosylases including hypoxanthine (repaired by MPG), 8oxoG:C lesion (repaired by OGG1, NEIL1, and NEIL2), and A:8oxoG lesion (repaired by MUTYH). pCX-NNX-D3GFP (a non-fluorescent protein expressing reporter plasmid) was used as a carrier plasmid to enhance the transfection efficiency. For each condition, cells were divided into 4 aliquots for transfection: 1) un-transfected cells; 2) transfection with undamaged plasmid cocktail; 3) transfection with damaged plasmid cocktail #1; 4.) transfection with damaged cocktail #2. The composition of each of the cocktails is given in Table 4.

Step 2: Transfection of cells with as-prepared reporter plasmids: The generic protocol for electroporation of mammalian cells with FM-HCR reporter plasmids has been described in a previous study of ours.[81] In brief, prior to electroporation, 24-well tissue culture plates with 800 μL per well /transfection of culture medium was placed into a 37°C incubator with 5% CO_2 for 10 mins. After incubation with ENMs, TK6 cells were centrifuged at 300g for 4 mins and the supernatant was carefully aspirated. The cell pellet was then resuspended in fresh, pre-equilibrated fully supplemented RPMI-1640 culture medium. 100 μL of cell suspension were aliquoted (untransfected, transfection with undamaged cocktail 1–2, transfection with damaged cocktail 1 and transfection with damaged cocktail 2) and then were mixed with the 1.5 μg of plasmid cocktail. Each aliquot was placed in the MXCell 96-well electroporation plate (Biorad, Cat no#1652681) and pulsed at 260V and 950 μF. Immediately after pulsing the cells, 100 μL of pre-warmed media was added into each of the pulsed wells and thoroughly mixed. The complete pulsed cell medium was transferred to the appropriate well in the 24-well plate and incubated for 24 hours at 37 °C and 5% CO_2. Post incubation, the cells were thoroughly resuspended and transferred to flow tubes for flow cytometry analysis.

SAEC at 60–70% confluency were plated in 12-well plates prior to exposure to ENMs. Post-exposure, the medium was aspirated from and fresh medium was added to the cells. LipofectamineTM 3000-based transfection was carried out following the manufacturer's guidelines (Thermofisher Scientific, Cat. #L3000001). In brief, after generating DNA-lipid complexes, 3.0 μg plasmid cocktail DNA was used added to SAECs and the plates were then incubated for 24 h at 37 °C incubator, 5% CO_2. Post-incubation, the medium was aliquoted in flow tubes. The cells were trypsinized using 400μl/well of trypsin for 4 mins and then culture medium containing serum was added to deactivate the trypsin. Trypsinized cells suspended in medium were added into the flow tube and proceeded for flow cytometry analysis.

Author Manuscript Author Manuscript Author Manuscript Author Manuscript

Step 3: Flow cytometry and analysis: 200ng of each fluorescent plasmid was transfected during each experiment of TK6 and SAECs which was used for single-color gating and compensation. The cells were collected after incubation and samples were processed by Attune NxT flow cytometry (Thermofisher Scientific). Doublets and higher order aggregates were excluded using forward *vs* side scatter. Singlet cells were gated to analyze the fluorescent reporter events. Data were analyzed in the Attune NxT software and Microsoft Excel following detailed analysis as described by Nagel *et al*.[81] Triplicate measurements were carried out for each condition. For quality control purposes, 10 fluorescent positive events and transfection efficiency above 0.1% was set as minimum threshold for data inclusion in our FM-HCR analysis. For each cocktail of plasmids, transfection efficiency was normalized to the transfection control. NHEJ, long patch BER and NER are reported as reporter expression (%) which equates to direct proportionality to repair capacity. Hx(MPG), 8oxoG:C and A:8oxoG reporter expression output from flow cytometry is inversely proportional to the repair capacity because they report the presence of the DNA lesion through transcriptional mutagenesis that occurs during lesion bypass by RNA polymerase. To represent data in an intuitive format where the reporter expression is directly proportional to DRC, we have computed the inverse of the reporter expression (1/reporter expression in %) for these plasmid readouts. The reporter expression from untreated cells was then normalized to reporter expression from treated cells of the same day to control for possible batch effects.

Statistical analyses.

For both the nano-CometChip assay and FM-HCR, one-way ANOVA analyses were used to compare statistical significance between the signals obtained from cells exposed to ENMs and control cells. Specifically, for the nano-CometChip assay, one-way ANOVA analysis with a Dunnett correction for multiple comparisons was used to test for significant differences between the cells exposed to ENMs *versus* control cells. For the FM-HCR assay, the raw fluorescent signals obtained from the internal transfection controls were used to normalize the fluorescent reporter expression for each plasmid. Then, the fluorescence signals from damaged plasmids in the ENM-treated cells were normalized against their undamaged counterparts and presented as percent reporter expression. Finally, percent reporter expression from the ENM exposed cells was normalized to percent reporter expression in untreated cells. The resulting normalized percent reporter expression signals were compared using a parametric unpaired t-test. Multiple comparisons between reporter plasmid expressions for different DNA repair pathways were considered independent, therefore statistical significance was set at $p \leq 0.05$. All statistical analyses were carried out on Prism 8.1.

Supplementary Material

Refer to Web version on PubMed Central for supplementary material.

Acknowledgments

Reported research has received support from the Nanyang Technological University-Harvard T. H. Chan School of Public Health Initiative for Sustainable Nanotechnology (NTU-Harvard SusNano; NTU-HSPH 18001). Engineered

Author Manuscript Author Manuscript Author Manuscript Author Manuscript

nanomaterials used in this research were synthesized and characterized by the Engineered Nanomaterials Resource and Coordination Core established at Harvard T.H. Chan School of Public Health (NIH grant # U24ES026946) as part of the Nanotechnology Health Implications Research (NHIR) Consortium. Z.D.N. and S.M.T were supported by U01ES029520. Partial funding for D.B. was provided by the International Initiative for the Environment and Public Health Cyprus Program of the Harvard School of Public Health. The authors would like to acknowledge the kind help of Prof B. Engelward with the nano-CometChip assay, and Prof G. Sotiriou and Padryk Merkl for the synthesis of Ga_2O_3 ENMs. The content is solely the responsibility of the authors and does not necessarily represent the official view of the National Institutes of Health.

References

1. Su H; Wang Y; Gu Y; Bowman L; Zhao J; Ding M Potential Applications and Human Biosafety of Nanomaterials Used in Nanomedicine. J. Appl. Toxicol 2018, 38 (1), 3–24. 10.1002/jat.3476. [PubMed: 28589558]
2. Huang R; Vaze N; Soorneedi A; Moore MD; Xue Y; Bello D; Demokritou P Inactivation of Hand Hygiene-Related Pathogens Using Engineered Water Nanostructures. ACS Sustain. Chem. Eng 2019, 7, 19761–19769. 10.1021/acssuschemeng.9b05057.
3. Bindraban PS; Dimkpa CO; White JC; Franklin FA; Melse-Boonstra A; Koele N; Pandey R; Rodenburg J; Senthilkumar K; Demokritou P; Schmidt S Safeguarding Human and Planetary Health Demands a Fertilizer Sector Transformation. PLANTS, PEOPLE, PLANET 2020, 2 (4), 302–309. 10.1002/ppp3.10098.
4. Vaze N; Pyrgiotakis G; Mena L; Baumann R; Demokritou A; Ericsson M; Zhang Y; Bello D; Eleftheriadou M; Demokritou P A Nano-Carrier Platform for the Targeted Delivery of Nature-Inspired Antimicrobials Using Engineered Water Nanostructures for Food Safety Applications. Food Control 2019, 96, 365–374. 10.1016/j.foodcont.2018.09.037. [PubMed: 32132770]
5. Rodrigues SM; Demokritou P; Dokoozlian N; Hendren CO; Karn B; Mauter MS; Sadik OA; Safarpour M; Unrine JM; Viers J; Welle P; White JC; Wiesner MR; Lowry GV Nanotechnology for Sustainable Food Production: Promising Opportunities and Scientific Challenges. Environ. Sci. Nano 2017, 4, 767–781. 10.1039/c6en00573j.
6. Eleftheriadou M; Pyrgiotakis G; Demokritou P Nanotechnology to the Rescue: Using Nano-Enabled Approaches in Microbiological Food Safety and Quality. Curr. Opin. Biotechnol 2017, 44, 87–93. 10.1016/j.copbio.2016.11.012. [PubMed: 27992831]
7. Xu T; Ma C; Aytac Z; Hu X; Ng KW; White JC; Demokritou P Enhancing Agrichemical Delivery and Seedling Development with Biodegradable, Tunable, Biopolymer-Based Nanofiber Seed Coatings. ACS Sustain. Chem. Eng 2020, 8 (25), 9537–9548. 10.1021/acssuschemeng.0c02696.
8. Gogotsi Y; Penner RM Energy Storage in Nanomaterials - Capacitive, Pseudocapacitive, or Battery-Like? ACS Nano 2018, 12 (3), 2081–2083. 10.1021/acsnano.8b01914. [PubMed: 29580061]
9. Singh D; Wohlleben W; De La Torre Roche R; White JC; Demokritou P Thermal Decomposition/ Incineration of Nano-Enabled Coatings and Effects of Nanofiller/Matrix Properties and Operational Conditions on Byproduct Release Dynamics: Potential Environmental Health Implications. NanoImpact 2019, 13 (September 2018), 44–55. 10.1016/j.impact.2018.12.003.
10. Zhang Q; Huang JQ; Qian WZ; Zhang YY; Wei F The Road for Nanomaterials Industry: A Review of Carbon Nanotube Production, Post-Treatment, and Bulk Applications for Composites and Energy Storage. Small 2013, 9 (8), 1237–1265. 10.1002/smll.201203252. [PubMed: 23580370]
11. Al-Jamal KT; Bai J; Wang JTW; Protti A; Southern P; Bogart L; Heidari H; Li X; Cakebread A; Asker D; Al-Jamal WT; Shah A; Bals S; Sosabowski J; Pankhurst QA Magnetic Drug Targeting: Preclinical *in Vivo* Studies, Mathematical Modeling, and Extrapolation to Humans. Nano Lett 2016, 16 (9), 5652–5660. 10.1021/acs.nanolett.6b02261. [PubMed: 27541372]
12. Sampathkumar K; Riyajan S; Tan CK; Demokritou P; Chudapongse N; Loo SCJ Small-Intestine-Specific Delivery of Antidiabetic Extracts from Withania Coagulans Using Polysaccharide-Based Enteric-Coated Nanoparticles. ACS Omega 2019, 4 (7), 12049–12057. 10.1021/acsomega.9b00823. [PubMed: 31460318]
13. Pyrgiotakis G; Luu W; Zhang Z; Vaze N; DeLoid G; Rubio L; Graham WAC; Bell DC; Bousfield D; Demokritou P Development of High Throughput, High Precision Synthesis Platforms and Characterization Methodologies for Toxicological Studies of Nanocellulose. Cellulose 2018, 25 (4), 2303–2319. 10.1007/s10570-018-1718-2. [PubMed: 31839698]

Author Manuscript Author Manuscript Author Manuscript Author Manuscript

14. Guo Z; Cao X; Deloid GM; Sampathkumar K; Ng KW; Loo SCJ; Demokritou P Physicochemical and Morphological Transformations of Chitosan Nanoparticles across the Gastrointestinal Tract and Cellular Toxicity in an *in Vitro* Model of the Small Intestinal Epithelium. J. Agric. Food Chem 2020, 68 (1), 358–368. 10.1021/acs.jafc.9b05506. [PubMed: 31815446]
15. Löbmann K; Svagan AJ Cellulose Nanofibers as Excipient for the Delivery of Poorly Soluble Drugs. Int. J. Pharm 2017, 533 (1), 285–297. 10.1016/j.ijpharm.2017.09.064. [PubMed: 28951349]
16. Khare S; DeLoid GM; Molina RM; Gokulan K; Couvillion SP; Bloodsworth KJ; Eder EK; Wong AR; Hoyt DW; Bramer LM; Metz TO; Thrall BD; Brain JD; Demokritou P Effects of Ingested Nanocellulose on Intestinal Microbiota and Homeostasis in Wistar Han Rats. NanoImpact 2020, 19, 1–12. 10.1016/j.impact.2020.100216.
17. Siddique R; Mehta A Effect of Carbon Nanotubes on Properties of Cement Mortars. Constr. Build. Mater 2014, 50, 116–129. 10.1016/j.conbuildmat.2013.09.019.
18. Bolotin KI; Ghahari F; Shulman MD; Stormer HL; Kim P Observation of the Fractional Quantum Hall Effect in Graphene. Nature 2009, 462, 196–199. 10.1038/nature08582. [PubMed: 19881489]
19. Sargent JF Jr Nanotechnology: A Policy Primer; Congressional Research Service, 2016.
20. Carll AP; Salatini R; Pirela SV; Wang Y; Xie Z; Lorkiewicz P; Naeem N; Qian Y; Castranova V; Godleski JJ; Demokritou P Inhalation of Printer-Emitted Particles Impairs Cardiac Conduction, Hemodynamics, and Autonomic Regulation and Induces Arrhythmia and Electrical Remodeling in Rats. Part. Fibre Toxicol 2020, 17 (7), 1–21. 10.1186/s12989-019-0335-z. [PubMed: 31900181]
21. Pirela SV; Lu X; Miousse I; Sisler JD; Qian Y; Guo N; Koturbash I; Castranova V; Thomas T; Godleski J; Demokritou P Effects of Intratracheally Instilled Laser Printer-Emitted Engineered Nanoparticles in a Mouse Model: A Case Study of Toxicological Implications from Nanomaterials Released during Consumer Use. NanoImpact 2016, 1, 1–8. 10.1016/j.impact.2015.12.001. [PubMed: 26989787]
22. Pirela SV; Martin J; Bello D; Demokritou P Nanoparticle Exposures from Nano-Enabled Toner-Based Printing Equipment and Human Health: State of Science and Future Research Needs. Crit. Rev. Toxicol 2017, 47 (8), 683–709. 10.1080/10408444.2017.1318354.
23. Weldon BA; Faustman EM; Oberdörster G; Workman T; Griffith WC; Kneuer C; Yu IJ Occupational Exposure Limit for Silver Nanoparticles: Considerations on the Derivation of a General Health-Based Value. Nanotoxicology 2016, 10 (7), 945–956. 10.3109/17435390.2016.1148793. [PubMed: 26982810]
24. Mackevica A; Olsson ME; Hansen SF The Release of Silver Nanoparticles from Commercial Toothbrushes. J. Hazard. Mater 2017, 322, 270–275. 10.1016/j.jhazmat.2016.03.067. [PubMed: 27045456]
25. Singh D; Sotiriou GA; Zhang F; Mead J; Bello D; Wohlleben W; Demokritou P End-of-Life Thermal Decomposition of Nano-Enabled Polymers: Effect of Nanofiller Loading and Polymer Matrix on By-Products. Environ. Sci. Nano 2016, 3, 1293–1305. 10.1039/c6en00252h.
26. Singh D; Schifman LA; Watson-Wright C; Sotiriou GA; Oyanedel-Craver V; Wohlleben W; Demokritou P Nanofiller Presence Enhances Polycyclic Aromatic Hydrocarbon (PAH) Profile on Nanoparticles Released during Thermal Decomposition of Nano-Enabled Thermoplastics: Potential Environmental Health Implications. Environ. Sci. Technol 2017, 51 (9), 5222–5232. 10.1021/acs.est.6b06448. [PubMed: 28397486]
27. Heller DA; Jena PV; Pasquali M; Kostarelos K; Delogu LG; Meidl RE; Rotkin SV; Scheinberg DA; Schwartz RE; Terrones M; Wang YH; Bianco A; Boghossian AA; Cambré S; Cognet L; Corrie SR; Demokritou P; Giordani S; Hertel T; Ignatova T et al. Banning Carbon Nanotubes Would Be Scientifically Unjustified and Damaging to Innovation. Nat. Nanotechnol 2020, 15, 164–166. 10.1038/s41565-020-0656-y.
28. Grassian VH; Haes AJ; Mudunkotuwa IA; Demokritou P; Kane AB; Murphy CJ; Hutchison JE; Isaacs JA; Jun YS; Karn B; Khondaker SI; Larsen SC; Lau BLT; Pettibone JM; Sadik OA; Saleh NB; Teague C NanoEHS - Defining Fundamental Science Needs: No Easy Feat When the Simple Itself Is Complex. Environ. Sci. Nano 2016, 3, 15–27. 10.1039/c5en00112a.
29. Parviz D; Bitounis D; Demokritou P; Strano M Engineering Two-Dimensional Nanomaterials to Enable Structure-Activity Relationship Studies in Nanosafety Research. NanoImpact 2020, 18, 1–9. 10.1016/j.impact.2020.100226.

Author Manuscript Author Manuscript Author Manuscript Author Manuscript

30. Sohal IS; O'Fallon KS; Gaines P; Demokritou P; Bello D Ingested Engineered Nanomaterials: State of Science in Nanotoxicity Testing and Future Research Needs. Part. Fibre Toxicol 2018, 15 (29), 1–31. 10.1186/s12989-018-0265-1. [PubMed: 29298690]

31. Duan Y; Coreas R; Liu Y; Bitounis D; Zhang Z; Parviz D; Strano M; Demokritou P; Zhong W Prediction of Protein Corona on Nanomaterials by Machine Learning Using Novel Descriptors. NanoImpact 2020, 17, 1–11. 10.1016/j.impact.2020.100207.

32. Evans SJ; Clift MJD; Singh N; De Oliveira Mallia J; Burgum M; Wills JW; Wilkinson TS; Jenkins GJS; Doak SH Critical Review of the Current and Future Challenges Associated with Advanced *in Vitro* Systems towards the Study of Nanoparticle (Secondary) Genotoxicity. Mutagenesis 2017, 32 (1), 233–241. 10.1093/mutage/gew054. [PubMed: 27815329]

33. Deloid GM; Cao X; Molina RM; Silva DI; Bhattacharya K; Ng KW; Loo SCJ; Brain JD; Demokritou P Toxicological Effects of Ingested Nanocellulose in *In Vitro* Intestinal Epithelium and *in Vivo* Rat Models. Environ. Sci. Nano 2019, 6, 2105–2115. 10.1039/c9en00184k. [PubMed: 32133146]

34. Tsuda A; Donaghey TC; Konduru NV; Pyrgiotakis G; Van Winkle LS; Zhang Z; Edwards P; Bustamante JM; Brain JD; Demokritou P Age-Dependent Translocation of Gold Nanoparticles across the Air-Blood Barrier. ACS Nano 2019, 13 (9), 10095–10102. 10.1021/acsnano.9b03019. [PubMed: 31397554]

35. Cao X; Deloid GMGM; Bitounis D; De La Torre-Roche R; White JCJC; Zhang Z; Ho CGCG; Ng KWKW; Eitzer BDBD; Demokritou P Co-Exposure to the Food Additives SiO2 (E551) or TiO2 (E171) and the Pesticide Boscalid Increases Cytotoxicity and Bioavailability of the Pesticide in a Tri-Culture Small Intestinal Epithelium Model: Potential Health Implications. Environ. Sci. Nano 2019, 6 (9), 2786–2800. 10.1039/c9en00676a. [PubMed: 32133147]

36. Kim S; Gates BL; Leonard BC; Gragg MM; Pinkerton KE; Van Winkle LS; Murphy CJ; Pyrgiotakis G; Zhang Z; Demokritou P; Thomasy SM Engineered Metal Oxide Nanomaterials Inhibit Corneal Epithelial Wound Healing *in Vitro* and *in Vivo*. NanoImpact 2020, 17, 1–10. 10.1016/j.impact.2019.100198.

37. Pietroiusti A; Campagnolo L; Fadeel B Interactions of Engineered Nanoparticles with Organs Protected by Internal Biological Barriers. Small 2013. 10.1002/smll.201201463.

38. Petters C; Thiel K; Dringen R Lysosomal Iron Liberation Is Responsible for the Vulnerability of Brain Microglial Cells to Iron Oxide Nanoparticles: Comparison with Neurons and Astrocytes. Nanotoxicology 2016, 10 (3), 332–342. 10.3109/17435390.2015.1071445. [PubMed: 26287375]

39. Wan R; Mo Y; Feng L; Chien S; Tollerud DJ; Zhang Q DNA Damage Caused by Metal Nanoparticles: Involvement of Oxidative Stress and Activation of ATM. Chem. Res. Toxicol 2012, 25 (7), 1402–1411. 10.1021/tx200513t. [PubMed: 22559321]

40. Sohal IS; DeLoid GM; O'Fallon KS; Gaines P; Demokritou P; Bello D Effects of Ingested Food-Grade Titanium Dioxide, Silicon Dioxide, Iron (III) Oxide and Zinc Oxide Nanoparticles on an *in Vitro* Model of Intestinal Epithelium: Comparison between Monoculture vs. a Mucus-Secreting Coculture Model. NanoImpact 2020, 17, 1–15. 10.1016/j.impact.2020.100209.

41. Touloumes GJ; Ardoña HAM; Casalino EK; Zimmerman JF; Chantre CO; Bitounis D; Demokritou P; Parker KK Mapping 2D- and 3D-Distributions of Metal/Metal Oxide Nanoparticles within Cleared Human *ex Vivo* Skin Tissues. NanoImpact 2020, 17, 1–11. 10.1016/j.impact.2020.100208.

42. Zhang Y; Demokritou P; Ryan DK; Bello D Comprehensive Assessment of Short-Lived ROS and H2O2 in Laser Printer Emissions: Assessing the Relative Contribution of Metal Oxides and Organic Constituents. Environ. Sci. Technol 2019, 53, 7574–7583. 10.1021/acs.est.8b05677. [PubMed: 31120250]

43. Rubio L; Pyrgiotakis G; Beltran-Huarac J; Zhang Y; Gaurav J; Deloid G; Spyrogianni A; Sarosiek KA; Bello D; Demokritou P Safer-by-Design Flame-Sprayed Silicon Dioxide Nanoparticles: The Role of Silanol Content on ROS Generation, Surface Activity and Cytotoxicity. Part. Fibre Toxicol 2019, 16 (40), 1–15. 10.1186/s12989-019-0325-1. [PubMed: 30612575]

44. Manke A; Wang L; Rojanasakul Y Mechanisms of Nanoparticle-Induced Oxidative Stress and Toxicity. Biomed Res. Int 2013, 2013, 1–15. 10.1155/2013/942916.

45. Dayem AA; Hossain MK; Lee S. Bin; Kim K; Saha SK; Yang GM; Choi HY; Cho SG The Role of Reactive Oxygen Species (ROS) in the Biological Activities of Metallic Nanoparticles. Int. J. Mol. Sci 2017, 18 (1), 1–21. 10.3390/ijms18010120.

Author Manuscript Author Manuscript Author Manuscript Author Manuscript

46. Nikjoo H; Emfietzoglou D; Liamsuwan T; Taleei R; Liljequist D; Uehara S Radiation Track, DNA Damage and Response - A Review. Reports Prog. Phys 2016, 79 (11), 1–55. 10.1088/0034-4885/79/11/116601.
47. Soren DC; Toprani SM; Jain V; Saini D; Das B Quantitation of Genome Damage and Transcriptional Profile of DNA Damage Response Genes in Human Peripheral Blood Mononuclear Cells Exposed *in Vitro* to Low Doses of Neutron Radiation. Int. J. Radiat. Res 2019, 17 (1), 1–14. 10.18869/acadpub.ijrr.17.1.1.
48. Masetti M; Xie HN; Krpetić Ž; Recanatini M; Alvarez-Puebla RA; Guerrini L Revealing DNA Interactions with Exogenous Agents by Surface-Enhanced Raman Scattering. J. Am. Chem. Soc 2015, 137 (1), 469–476. 10.1021/ja511398w. [PubMed: 25496029]
49. De Bont R; van Larebeke N Endogenous DNA Damage in Humans: A Review of Quantitative Data. Mutagenesis 2004, 19 (3), 169–185. 10.1093/mutage/geh025. [PubMed: 15123782]
50. Gonzalez L; Lison D; Kirsch-Volders M Genotoxicity of Engineered Nanomaterials: A Critical Review. Nanotoxicology 2008, 2 (5), 252–273. 10.1080/17435390802464986.
51. Singh N; Nelson BC; Scanlan LD; Coskun E; Jaruga P; Doak SH Exposure to Engineered Nanomaterials: Impact on DNA Repair Pathways. Int. J. Mol. Sci 2017, 18 (7), 1–15. 10.3390/ijms18071515.
52. Biola-Clier M; Beal D; Caillat S; Libert S; Armand L; Herlin-Boime N; Sauvaigo S; Douki T; Carriere M Comparison of the DNA Damage Response in BEAS-2B and A549 Cells Exposed to Titanium Dioxide Nanoparticles. Mutagenesis 2017, 32 (1), 161–172. 10.1093/mutage/gew055. [PubMed: 27803034]
53. Lu X; Miousse IR; Pirela SV; Melnyk S; Koturbash I; Demokritou P Short-Term Exposure to Engineered Nanomaterials Affects Cellular Epigenome. Nanotoxicology 2016, 10 (2), 140–150. 10.3109/17435390.2015.1025115. [PubMed: 25938281]
54. Lu X; Miousse IR; Pirela SV; Moore JK; Melnyk S; Koturbash I; Demokritou P *In Vivo* Epigenetic Effects Induced by Engineered Nanomaterials: A Case Study of Copper Oxide and Laser Printer-Emitted Engineered Nanoparticles. Nanotoxicology 2016, 10 (5), 629–639. 10.3109/17435390.2015.1108473. [PubMed: 26559097]
55. Errol CF; Graham CW; Wolfram S; Richard DW; Roger AS; Tom E DNA Repair and Mutagenesis, Second Edition; 2006. 10.1128/9781555816704.
56. Milanowska K; Krwawicz J; Papaj G; Kosiński J; Poleszak K; Lesiak J; Osińska E; Rother K; Bujnicki JM REPAIRtoire-A Database of DNA Repair Pathways. Nucleic Acids Res 2011, 39, 788–792. 10.1093/nar/gkq1087.
57. Sun T; Yang W; Toprani SM; Guo W; He L; Deleo AB; Ferrone S; Zhang G; Wang E; Lin Z; Hu P; Wang X Induction of Immunogenic Cell Death in Radiation-Resistant Breast Cancer Stem Cells by Repurposing Anti-Alcoholism Drug Disulfiram. Cell Commun. Signal 2020, 18 (3), 1–14. 10.1186/s12964-019-0507-3. [PubMed: 31900175]
58. Nagel ZD; Chaim IA; Samson LD Inter-Individual Variation in DNA Repair Capacity: A Need for Multi-Pathway Functional Assays to Promote Translational DNA Repair Research. DNA Repair (Amst) 2014, 19, 199–213. 10.1016/j.dnarep.2014.03.009. [PubMed: 24780560]
59. Toprani SM; Das B Role of Base Excision Repair Genes and Proteins in Gamma-Irradiated Resting Human Peripheral Blood Mononuclear Cells. Mutagenesis 2015, 30 (2), 247–261. 10.1093/mutage/geu065. [PubMed: 25381310]
60. Toprani SM; Kelkar Mane V Role of DNA Damage and Repair Mechanisms in Uterine Fibroid/Leiomyomas: A Review. Biol. Reprod 2020, 104 (1), 58–70. 10.1093/biolre/ioaa157.
61. Toprani SM; Das B Radio-Adaptive Response, Individual Radio-Sensitivity and Correlation of Base Excision Repair Gene Polymorphism (HOGG1, APE1, XRCC1, and LIGASE1) in Human Peripheral Blood Mononuclear Cells Exposed to Gamma Radiation. Environ. Mol. Mutagen 2020, 61 (5), 551–559. 10.1002/em.22383. [PubMed: 32324932]
62. Chatterjee N; Walker GC Mechanisms of DNA Damage, Repair, and Mutagenesis. Environ. Mol. Mutagen 2017, 58 (5), 235–263. 10.1002/em.22087. [PubMed: 28485537]
63. Zhao B; Rothenberg E; Ramsden DA; Lieber MR The Molecular Basis and Disease Relevance of Non-Homologous DNA End Joining. Nat. Rev. Mol. Cell Biol 2020, 21, 765–781. 10.1038/s41580-020-00297-8. [PubMed: 33077885]

Author Manuscript Author Manuscript Author Manuscript Author Manuscript

64. Nagel ZD; Engelward BP; Brenner DJ; Begley TJ; Sobol RW; Bielas JH; Stambrook PJ; Wei Q; Hu JJ; Terry MB; Dilworth C; McAllister KA; Reinlib L; Worth L; Shaughnessy DT Towards Precision Prevention: Technologies for Identifying Healthy Individuals with High Risk of Disease. Mutat. Res. - Fundam. Mol. Mech. Mutagen 2017, 800–802, 14–28. 10.1016/j.mrfmmm.2017.03.007.

65. Toprani SM; Das B Radio-Adaptive Response of Base Excision Repair Genes and Proteins in Human Peripheral Blood Mononuclear Cells Exposed to Gamma Radiation. Mutagenesis 2015, 30 (5), 663–676. 10.1093/mutage/gev032. [PubMed: 25958388]

66. Broustas CG; Lieberman HB DNA Damage Response Genes and the Development of Cancer Metastasis. Radiat. Res 2014, 181 (2), 111–130. 10.1667/rr13515.1. [PubMed: 24397478]

67. Toprani SM DNA Damage and Repair Scenario in Ameloblastoma. Oral Oncol 2020, 108, 1–5. 10.1016/j.oraloncology.2020.104804.

68. Cadet J; Douki T; Ravanat JL Oxidatively Generated Damage to Cellular DNA by UVB and UVA Radiation. Photochem. Photobiol 2015, 91 (1), 140–155. 10.1111/php.12368. [PubMed: 25327445]

69. Watson C; Ge J; Cohen J; Pyrgiotakis G; Engelward BP; Demokritou P High-Throughput Screening Platform for Engineered Nanoparticle-Mediated Genotoxicity Using Cometchip Technology. ACS Nano 2014, 8 (3), 2118–2133. 10.1021/nn404871p. [PubMed: 24617523]

70. El-Said KS; Ali EM; Kanehira K; Taniguchi A Molecular Mechanism of DNA Damage Induced by Titanium Dioxide Nanoparticles in Toll-Like Receptor 3 or 4 Expressing Human Hepatocarcinoma Cell Lines. J. Nanobiotechnology 2014, 12 (48), 1–10. 10.1186/s12951-014-0048-2. [PubMed: 24411017]

71. Khatri M; Bello D; Pal AK; Cohen JM; Woskie S; Gassert T; Lan J; Gu AZ; Demokritou P; Gaines P Evaluation of Cytotoxic, Genotoxic and Inflammatory Responses of Nanoparticles from Photocopiers in Three Human Cell Lines. Part. Fibre Toxicol 2013, 10 (42), 1–22. 10.1186/1743-8977-10-42. [PubMed: 23305071]

72. Tang S; Wu Y; Ryan CN; Yu S; Qin G; Edwards DS; Mayer GD Distinct Expression Profiles of Stress Defense and DNA Repair Genes in Daphnia Pulex Exposed to Cadmium, Zinc, and Quantum Dots. Chemosphere 2015, 120, 92–99. 10.1016/j.chemosphere.2014.06.011. [PubMed: 25014899]

73. Tang S; Cai Q; Chibli H; Allagadda V; Nadeau JL; Mayer GD Cadmium Sulfate and CdTe-Quantum Dots Alter DNA Repair in Zebrafish (Danio rerio) Liver Cells. Toxicol. Appl. Pharmacol 2013, 272 (2), 443–452. 10.1016/j.taap.2013.06.004. [PubMed: 23770381]

74. van Berlo D; Hullmann M; Wessels A; Scherbart AM; Cassee FR; Gerlofs-Nijland ME; Albrecht C; Schins RPF Investigation of the Effects of Short-Term Inhalation of Carbon Nanoparticles on Brains and Lungs of C57bl/6j and P47phox−/− Mice. Neurotoxicology 2014, 43, 65–72. 10.1016/j.neuro.2014.04.008. [PubMed: 24792328]

75. Asare N; Duale N; Slagsvold HH; Lindeman B; Olsen AK; Gromadzka-Ostrowska J; Meczynska-Wielgosz S; Kruszewski M; Brunborg G; Instanes C Genotoxicity and Gene Expression Modulation of Silver and Titanium Dioxide Nanoparticles in Mice. Nanotoxicology 2016, 10 (3), 312–321. 10.3109/17435390.2015.1071443. [PubMed: 26923343]

76. Kovvuru P; Mancilla PE; Shirode AB; Murray TM; Begley TJ; Reliene R Oral Ingestion of Silver Nanoparticles Induces Genomic Instability and DNA Damage in Multiple Tissues. Nanotoxicology 2015, 9 (2), 161–171. 10.3109/17435390.2014.902520.

77. Ahamed M; Siddiqui MA; Akhtar MJ; Ahmad I; Pant AB; Alhadlaq HA Genotoxic Potential of Copper Oxide Nanoparticles in Human Lung Epithelial Cells. Biochem. Biophys. Res. Commun 2010, 2, 578–583. 10.1016/j.bbrc.2010.04.156.

78. Pati R; Das I; Mehta RK; Sahu R; Sonawane A Zinc-Oxide Nanoparticles Exhibit Genotoxic, Clastogenic, Cytotoxic and Actin Depolymerization Effects by Inducing Oxidative Stress Responses in Macrophages and Adult Mice. Toxicol. Sci 2016, 150 (2), 454–472. 10.1093/toxsci/kfw010. [PubMed: 26794139]

79. Hanot-Roy M; Tubeuf E; Guilbert A; Bado-Nilles A; Vigneron P; Trouiller B; Braun A; Lacroix G Oxidative Stress Pathways Involved in Cytotoxicity and Genotoxicity of Titanium Dioxide (TiO2) Nanoparticles on Cells Constitutive of Alveolo-Capillary Barrier *in Vitro*. Toxicol. Vitr 2016, 33, 125–135. 10.1016/j.tiv.2016.01.013.

Author Manuscript Author Manuscript Author Manuscript Author Manuscript

80. Prasad RY; Chastain PD; Nikolaishvili-Feinberg N; Smeester L; Kaufmann WK; Fry RC Titanium Dioxide Nanoparticles Activate the ATM-Chk2 DNA Damage Response in Human Dermal Fibroblasts. Nanotoxicology 2013, 7 (6), 1111–1119. 10.3109/17435390.2012.710659. [PubMed: 22770119]
81. Nagel ZD; Margulies CM; Chaim IA; McRee SK; Mazzucato P; Ahmad A; Abo RP; Butty VL; Forget AL; Samson LD Multiplexed DNA Repair Assays for Multiple Lesions and Multiple Doses *via* Transcription Inhibition and Transcriptional Mutagenesis. Proc. Natl. Acad. Sci. U. S. A 2014, 111, 1823–1832. 10.1073/pnas.1401182111.
82. Chaim IA; Nagel ZD; Jordan JJ; Mazzucato P; Ngo LP; Samson LD *In Vivo* Measurements of Interindividual Differences in DNA Glycosylases and APE1 Activities. Proc. Natl. Acad. Sci. U. S. A 2017, 114, 10379–10388. 10.1073/pnas.1712032114. [PubMed: 28900003]
83. Beharry AA; Nagel ZD; Samson LD; Kool ETK Fluorogenic Real-Time Reporters of DNA Repair by MGMT, a Clinical Predictor of Antitumor Drug Response. PLoS One 2016, 11 (4), 15. 10.1371/journal.pone.0152684.
84. Pal AK; Bello D; Cohen J; Demokritou P Implications of *in Vitro* Dosimetry on Toxicological Ranking of Low Aspect Ratio Engineered Nanomaterials. Nanotoxicology 2015, 9 (7), 871–885. 10.3109/17435390.2014.986670. [PubMed: 25672815]
85. Cohen JM; Teeguarden JG; Demokritou P An Integrated Approach for the *in Vitro* Dosimetry of Engineered Nanomaterials. Part. Fibre Toxicol 2014, 11 (20), 1–12. 10.1186/1743-8977-11-20. [PubMed: 24382024]
86. Cohen JM; Beltran-Huarac J; Pyrgiotakis G; Demokritou P Effective Delivery of Sonication Energy to Fast Settling and Agglomerating Nanomaterial Suspensions for Cellular Studies: Implications for Stability, Particle Kinetics, Dosimetry and Toxicity. NanoImpact 2018, 10, 81–86. 10.1016/j.impact.2017.12.002. [PubMed: 29479575]
87. DeLoid GM; Cohen JM; Pyrgiotakis G; Demokritou P Preparation, Characterization, and *in Vitro* Dosimetry of Dispersed, Engineered Nanomaterials. Nat. Protoc 2017, 12 (2), 355–371. 10.1038/nprot.2016.172. [PubMed: 28102836]
88. Deloid G; Cohen JM; Darrah T; Derk R; Rojanasakul L; Pyrgiotakis G; Wohlleben W; Demokritou P Estimating the Effective Density of Engineered Nanomaterials for *in Vitro* Dosimetry. Nat. Commun 2014, 5 (3513), 1–10. 10.1038/ncomms4514.
89. Adar S; Hu J; Lieb JD; Sancar A Genome-Wide Kinetics of DNA Excision Repair in Relation to Chromatin State and Mutagenesis. Proc. Natl. Acad. Sci. U. S. A 2016, 113 (15), 2124–2133. 10.1073/pnas.1603388113.
90. Kim JA; Aberg C; Salvati A; Dawson KA Role of Cell Cycle on the Cellular Uptake and Dilution of Nanoparticles in a Cell Population. Nat. Nanotechnol 2012, 7, 62–68. 10.1038/nnano.2011.191.
91. Akerman GS; Rosenzweig BA; Domon OE; Tsai C; Bishop ME; McGarrity LJ; MacGregor JT; Sistare FD; Chen JJ; Morris SM Alterations in Gene Expression Profiles and the DNA-damage Response in Ionizing Radiation-exposed TK6 Cells. Environ. Mol. Mutagen 2005, 45 (2-3), 188–205. [PubMed: 15657912]
92. Pirela SV; Miousse IR; Lu X; Castranova V; Thomas T; Qian Y; Bello D; Kobzik L; Koturbash I; Demokritou P Effects of Laser Printer–Emitted Engineered Nanoparticles on Cytotoxicity, Chemokine Expression, Reactive Oxygen Species, DNA Methylation, and DNA Damage: A Comprehensive *in Vitro* Analysis in Human Small Airway Epithelial Cells, Macrophages, and Lymphobla. Environ. Health Perspect 2016, 124 (2), 210–219. 10.1289/ehp.1409582. [PubMed: 26080392]
93. Wu Z; Shi P; Lim HK; Ma Y; Setyawati MI; Bitounis D; Demokritou P; Ng KW; Tay CY Inflammation Increases Susceptibility of Human Small Airway Epithelial Cells to Pneumonic Nanotoxicity. Small 2020, 16 (21), 1–7. 10.1002/smll.202000963.
94. Han G; Martin CT; Rotello VM Stability of Gold Nanoparticle-Bound DNA toward Biological, Physical, and Chemical Agents. Chem. Biol. Drug Des 2006, 67 (1), 78–82. 10.1111/j.1747-0285.2005.00324.x. [PubMed: 16492152]
95. Liu Y; Zhong R; Zhang P; Ma Y; Yun X; Gong P; Wei J; Zhao X; Zhang F Understanding the Robust Physisorption between Bovine Serum Albumin and Amphiphilic Polymer Coated Nanoparticles. ACS Appl. Mater. Interfaces 2016, 8 (4), 2478–2485. 10.1021/acsami.5b08386. [PubMed: 26718324]

Author Manuscript Author Manuscript Author Manuscript Author Manuscript

96. Leung KCF; Chak CP; Lee SF; Lai JMY; Zhu XM; Wang YXJ; Sham KWY; Cheng CHK Enhanced Cellular Uptake and Gene Delivery of Glioblastoma with Deferoxamine-Coated Nanoparticle/Plasmid DNA/Branched Polyethylenimine Composites. Chem. Commun 2013, 49, 549–551. 10.1039/c2cc36663k.

97. van der Pol E; Coumans FAW; Grootemaat AE; Gardiner C; Sargent IL; Harrison P; Sturk A; van Leeuwen TG; Nieuwland R Particle Size Distribution of Exosomes and Microvesicles Determined by Transmission Electron Microscopy, Flow Cytometry, Nanoparticle Tracking Analysis, and Resistive Pulse Sensing. J. Thromb. Haemost 2014, 12 (7), 1182–1192. 10.1111/jth.12602. [PubMed: 24818656]

98. van Gaal EVB; Spierenburg G; Hennink WE; Crommelin DJA; Mastrobattista E Flow Cytometry for Rapid Size Determination and Sorting of Nucleic Acid Containing Nanoparticles in Biological Fluids. J. Control. Release 2010, 141 (3), 328–338. 10.1016/j.jconrel.2009.09.009. [PubMed: 19778559]

99. Eweje F; Ardonã HAMHAM; Zimmerman JFJF; O'Connor BBB; Ahn S; Grevesse T; Rivera KNKN; Bitounis D; Demokritou P; Parker KK K. K. Quantifying the Effects of Engineered Nanomaterials on Endothelial Cell Architecture and Vascular Barrier Integrity Using a Cell Pair Model. Nanoscale 2019, 11 (38), 17878–17893. 10.1039/c9nr04981a. [PubMed: 31553035]

100. Flynn H; Hwang D; Holman M Nanotechnology Update: Corporations up Their Spending as Revenues for Nano-Enabled Products Increase 2017.

101. Branica G; Mladinić M; Omanović D; Želježić D An Alternative Approach to Studying the Effects of ZnO Nanoparticles in Cultured Human Lymphocytes: Combining Electrochemistry and Genotoxicity Tests. Arh. Hig. Rada Toksikol 2016, 67 (41), 277–288. 10.1515/aiht-2016-67-2910. [PubMed: 28033099]

102. Thomas AD; Fahrer J; Johnson GE; Kaina B Theoretical Considerations for Thresholds in Chemical Carcinogenesis. Mutat. Res. - Rev. Mutat. Res 2015, 765, 56–67. 10.1016/j.mrrev.2015.05.001. [PubMed: 26281768]

103. Sevilya Z; Leitner-Dagan Y; Pinchev M; Kremer R; Elinger D; Rennert HS; Schechtman E; Freedman LS; Rennert G; Paz-Elizur T; Livneh Z Low Integrated DNA Repair Score and Lung Cancer Risk. Cancer Prev. Res 2014, 7 (4), 398–406. 10.1158/1940-6207.CAPR-13-0318.

104. Posnick LM; Samson LD Imbalanced Base Excision Repair Increases Spontaneous Mutation and Alkylation Sensitivity in Escherichia Coli. J. Bacteriol 1999, 181 (21), 6763–6771. 10.1128/jb.181.21.6763-6771.1999. [PubMed: 10542179]

105. Aardema MJ The Holy Grail in Genetic Toxicology: Follow-Up Approaches for Positive Results in the Ames Assay. Environ. Mol. Mutagen 2013, 54 (8), 617–620. 10.1002/em.21813. [PubMed: 24108513]

106. Demir E; Creus A; Marcos R Genotoxicity and DNA Repair Processes of Zinc Oxide Nanoparticles. J. Toxicol. Environ. Heal. - Part A Curr. Issues 2014, 77 (21), 1292–1303. 10.1080/15287394.2014.935540.

107. Valdiglesias V; Costa C; Kiliç G; Costa S; Pásaro E; Laffon B; Teixeira JP Neuronal Cytotoxicity and Genotoxicity Induced by Zinc Oxide Nanoparticles. Environ. Int 2013, 55, 92–100. 10.1016/j.envint.2013.02.013. [PubMed: 23535050]

108. Zijno A; De Angelis I; De Berardis B; Andreoli C; Russo MT; Pietraforte D; Scorza G; Degan P; Ponti J; Rossi F; Barone F Different Mechanisms Are Involved in Oxidative DNA Damage and Genotoxicity Induction by ZnO and TiO2 Nanoparticles in Human Colon Carcinoma Cells. Toxicol. Vitr 2015, 29 (7), 1503–1512. 10.1016/j.tiv.2015.06.009.

109. Hartmann A; Speit G Effect of Arsenic and Cadmium on the Persistence of Mutagen-Induced DNA Lesions in Human Cells. Environ. Mol. Mutagen 1996, 27 (2), 98–104. 10.1002/(SICI)1098-2280(1996)27:2<98::AID-EM4>3.0.CO;2-A. [PubMed: 8603672]

110. Wolff S The Adaptive Response in Radiobiology: Evolving Insights and Implications. Environ. Health Perspect 1998, 106, 277–283. 10.2307/3433927. [PubMed: 9539019]

111. Huang YW; Cambre M; Lee HJ The Toxicity of Nanoparticles Depends on Multiple Molecular and Physicochemical Mechanisms. Int. J. Mol. Sci 2017, 18 (12), 1–13. 10.3390/ijms18122702.

Author Manuscript Author Manuscript Author Manuscript Author Manuscript

112. Chakraborty S; Nair A; Paliwal M; Dybowska A; Misra SK Exposure Media a Critical Factor for Controlling Dissolution of CuO Nanoparticles. J. Nanoparticle Res 2018, 20 (12), 1–14. 10.1007/s11051-018-4428-7.

113. Rochester JR Bisphenol A and Human Health: A Review of the Literature. Reprod. Toxicol 2013, 42, 132–155. 10.1016/j.reprotox.2013.08.008. [PubMed: 23994667]

114. Williams AB; Schumacher B P53 in the DNA-Damage-Repair Process; 2016. 10.1101/cshperspect.a026070.

115. Oka S; Leon J; Tsuchimoto D; Sakumi K; Nakabeppu Y MUTYH, an Adenine DNA Glycosylase, Mediates P53 Tumor Suppression via PARP-Dependent Cell Death. Oncogenesis 2014, 3, 1–10. 10.1038/oncsis.2014.35.

116. Chatterjee A; Mambo E; Osada M; Upadhyay S; Sidransky D The Effect of P53-RNAi and P53 Knockout on Human 8-oxoguanine DNA Glycosylase (HOgg1) Activity. FASEB J 2006, 20 (1), 112–114. 10.1096/fj.04-3423fje. [PubMed: 16293709]

117. Zaky A; Busso C; Izumi T; Chattopadhyay R; Bassiouny A; Mitra S; Bhakat KK Regulation of the Human AP-Endonuclease (APE1/Ref-1) Expression by the Tumor Suppressor P53 in Response to DNA Damage. Nucleic Acids Res 2008, 36 (5), 1555–1566. [PubMed: 18208837]

118. Semisch A; Ohle J; Witt B; Hartwig A Cytotoxicity and Genotoxicity of Nano - And Microparticulate Copper Oxide: Role of Solubility and Intracellular Bioavailability. Part. Fibre Toxicol 2014, 11 (10), 1–16. 10.1186/1743-8977-11-10. [PubMed: 24382024]

119. Zimmerman JF; Ardoña HAM; Pyrgiotakis G; Dong J; Moudgil B; Demokritou P; Parker KK Scatter Enhanced Phase Contrast Microscopy for Discriminating Mechanisms of Active Nanoparticle Transport in Living Cells. Nano Lett 2019, 19 (2), 793–804. 10.1021/acs.nanolett.8b03903. [PubMed: 30616354]

120. Tsuda A; Konduru NV The Role of Natural Processes and Surface Energy of Inhaled Engineered Nanoparticles on Aggregation and Corona Formation. NanoImpact 2016, 2, 38–44. 10.1016/j.impact.2016.06.002. [PubMed: 29202111]

121. Konduru NV; Molina RM; Swami A; Damiani F; Pyrgiotakis G; Lin P; Andreozzi P; Donaghey TC; Demokritou P; Krol S; Kreyling W; Brain JD Protein Corona: Implications for Nanoparticle Interactions with Pulmonary Cells. Part. Fibre Toxicol 2017, 14 (42), 1–12. 10.1186/s12989-017-0223-3. [PubMed: 28069023]

122. Faria M; Björnmalm M; Thurecht KJ; Kent SJ; Parton RG; Kavallaris M; Johnston APR; Gooding JJ; Corrie SR; Boyd BJ; Thordarson P; Whittaker AK; Stevens MM; Prestidge CA; Porter CJH; Parak WJ; Davis TP; Crampin EJ; Caruso F Minimum Information Reporting in Bio–Nano Experimental Literature. Nat. Nanotechnol 2018, 13, 777–785. 10.1038/s41565-018-0246-4. [PubMed: 30190620]

123. Hintzsche H; Montag G; Stopper H Induction of Micronuclei by Four Cytostatic Compounds in Human Hematopoietic Stem Cells and Human Lymphoblastoid TK6 Cells. Sci. Rep 2018, 8, 1–11. 10.1038/s41598-018-21680-8. [PubMed: 29311619]

124. Behzadi S; Serpooshan V; Tao W; Hamaly MA; Alkawareek MY; Dreaden EC; Brown D; Alkilany AM; Farokhzad OC; Mahmoudi M Cellular Uptake of Nanoparticles: Journey inside the Cell. Chem. Soc. Rev 2017, 46, 4218–4244. 10.1039/c6cs00636a. [PubMed: 28585944]

125. Sobolt RW; Kartalou M; Almeida KH; Joyce DF; Engelward BP; Horton JK; Prasad R; Samson LD; Wilson SH Base Excision Repair Intermediates Induce P53-Independent Cytotoxic and Genotoxic Responses. J. Biol. Chem 2003, 278 (41), 39951–39959. 10.1074/jbc.M306592200. [PubMed: 12882965]

126. Delaney JC; Essigmann JM Biological Properties of Single Chemical-DNA Adducts: A Twenty Year Perspective. Chem. Res. Toxicol 2008, 21 (1), 232–252. 10.1021/tx700292a. [PubMed: 18072751]

127. Maynard S; Fang EF; Scheibye-Knudsen M; Croteau DL; Bohr VA DNA Damage, DNA Repair, Aging, and Neurodegeneration. Cold Spring Harb. Perspect. Med 2015, 5 (10), 1–18. 10.1101/cshperspect.a025130.

128. Verheijen BM; van Leeuwen FW Commentary: The Landscape of Transcription Errors in Eukaryotic Cells. Front. Genet 2017, 8 (219), 1–4. 10.3389/fgene.2017.00219. [PubMed: 28179914]

Author Manuscript Author Manuscript Author Manuscript Author Manuscript

129. Annangi B; Rubio L; Alaraby M; Bach J; Marcos R; Hernández A Acute and Long-Term *in Vitro* Effects of Zinc Oxide Nanoparticles. Arch. Toxicol 2016, 90 (9), 2201–2213. 10.1007/s00204-015-1613-7. [PubMed: 26449478]

130. Demokritou P; Büchel R; Molina RM; Deloid GM; Brain JD; Pratsinis SE Development and Characterization of a Versatile Engineered Nanomaterial Generation System (VENGES) Suitable for Toxicological Studies. Inhal. Toxicol 2010, 22 (sup2), 107–116. [PubMed: 20701428]

131. Beltran-Huarac J; Zhang Z; Pyrgiotakis G; DeLoid G; Vaze N; Demokritou P Development of Reference Metal and Metal Oxide Engineered Nanomaterials for Nanotoxicology Research Using High Throughput and Precision Flame Spray Synthesis Approaches. NanoImpact 2018, 10, 26–37. 10.1016/j.impact.2017.11.007. [PubMed: 30035243]

132. Mädler L; Kammler HK; Mueller R; Pratsinis SE Controlled Synthesis of Nanostructured Particles by Flame Spray Pyrolysis. J. Aerosol Sci 2002, 33 (2), 369–389. 10.1016/S0021-8502(01)00159-8.

133. DeLoid GM; Cohen JM; Pyrgiotakis G; Pirela SV; Pal A; Liu J; Srebric J; Demokritou P Advanced Computational Modeling for *in Vitro* Nanomaterial Dosimetry. Part. Fibre Toxicol 2015, 12 (32), 1–20. 10.1186/s12989-015-0109-1. [PubMed: 25605549]

134. Wilson DM; Bohr VA The Mechanics of Base Excision Repair, and Its Relationship to Aging and Disease. DNA Repair (Amst) 2007, 6 (4), 544–559. 10.1016/j.dnarep.2006.10.017. [PubMed: 17112792]

135. Weissman L; Jo DG; Sørensen MM; de Souza-Pinto NC; Markesbery WR; Mattson MP; Bohr VA Defective DNA Base Excision Repair in Brain from Individuals with Alzheimer's Disease and Amnestic Mild Cognitive Impairment. Nucleic Acids Res 2007, 35 (26), 5545–5555. 10.1093/nar/gkm605. [PubMed: 17704129]

136. Krokan HE; Bjørås M Base Excision Repair; 2013. 10.1101/cshperspect.a012583.

137. Bosshard M; Markkanen E; van Loon B Base Excision Repair in Physiology and Pathology of the Central Nervous System. Int. J. Mol. Sci 2012, 13 (12), 16172–16222. 10.3390/ijms131216172. [PubMed: 23203191]

138. Karahalil B; Bohr VA; Wilson DM Impact of DNA Polymorphisms in Key DNA Base Excision Repair Proteins on Cancer Risk. Hum. Exp. Toxicol 2012, 31 (10), 981–1005. 10.1177/0960327112444476. [PubMed: 23023028]

139. Berndt SI; Huang WY; Fallin MD; Helzlsouer KJ; Platz EA; Weissfeld JL; Church TR; Welch R; Chanock SJ; Hayes RB Genetic Variation in Base Excision Repair Genes and the Prevalence of Advanced Colorectal Adenoma. Cancer Res 2007, 67 (3), 1395–1404. 10.1158/0008-5472.CAN-06-1390. [PubMed: 17283177]

140. Sepe S; Milanese C; Gabriels S; Derks KWJ; Payan-Gomez C; van IJcken WFJ; Rijksen YMA; Nigg AL; Moreno S; Cerri S; Blandini F; Hoeijmakers JHJ; Mastroberardino PG Inefficient DNA Repair Is an Aging-Related Modifier of Parkinson's Disease. Cell Rep 2016, 15 (9), 1866–1875. 10.1016/j.celrep.2016.04.071. [PubMed: 27210754]

141. Busch D; Greiner C; Lewis K; Ford R; Adair G; Thompson L Summary of Complementation Groups of UV-Sensitive CHO Cell Mutants Isolated by Large-Scale Screening. Mutagenesis 1989, 4 (5), 349–354. 10.1093/mutage/4.5.349. [PubMed: 2687628]

142. Kwon HC; Roh MS; Oh SY; Kim SH; Kim MC; Kim JS; Kim HJ Prognostic Value of Expression of ERCC1, Thymidylate Synthase, and Glutathione S-Transferase P1 for 5-Fluorouracil/Oxaliplatin Chemotherapy in Advanced Gastric Cancer. Ann. Oncol 2007, 18, 504–509. 10.1093/annonc/mdl430. [PubMed: 17322540]

143. Bellmunt J; Paz-Ares L; Cuello M; Cecere FL; Albiol S; Guillem V; Gallardo E; Carles J; Mendez P; de la Cruz JJ; Taron M; Rosell R; Baselga J Gene Expression of ERCC1 as a Novel Prognostic Marker in Advanced Bladder Cancer Patients Receiving Cisplatin-Based Chemotherapy. Ann. Oncol 2007, 3, 522–528. 10.1093/annonc/mdl435.

144. Wang XS; Lee BJ; Zha S The Recent Advances in Non-Homologous End-Joining through the Lens of Lymphocyte Development. DNA Repair (Amst) 2020, 94, 1–12. 10.1016/j.dnarep.2020.102874.

Author Manuscript Author Manuscript Author Manuscript Author Manuscript

145. Du W; Amarachintha S; Wilson AF; Pang Q Hyper-Active Non-Homologous End Joining Selects for Synthetic Lethality Resistant and Pathological Fanconi Anemia Hematopoietic Stem and Progenitor Cells. Sci. Rep 2016, 6, 1–12. 10.1038/srep22167. [PubMed: 28442746]

146. Fishel ML; Seo YR; Smith ML; Kelley MR Imbalancing the DNA Base Excision Repair Pathway in the Mitochondria; Targeting and Overexpressing N-Methylpurine DNA Glycosylase in Mitochondria Leads to Enhanced Cell Killing. Cancer Res 2003, 63 (3), 608–615. [PubMed: 12566303]

147. Crosbie PAJ; Watson AJ; Agius R; Barber PV; Margison GP; Povey AC Elevated N3-Methylpurine-DNA Glycosylase DNA Repair Activity Is Associated with Lung Cancer. Mutat. Res. - Fundam. Mol. Mech. Mutagen 2012, 732, 43–46. 10.1016/j.mrfmmm.2012.01.001.

148. Fleming AM; Ding Y; Burrows CJ Oxidative DNA Damage Is Epigenetic by Regulating Gene Transcription *via* Base Excision Repair. Proc. Natl. Acad. Sci. U. S. A 2017, 114 (10), 2604–2609. 10.1073/pnas.1619809114. [PubMed: 28143930]

Author Manuscript Author Manuscript Author Manuscript Author Manuscript

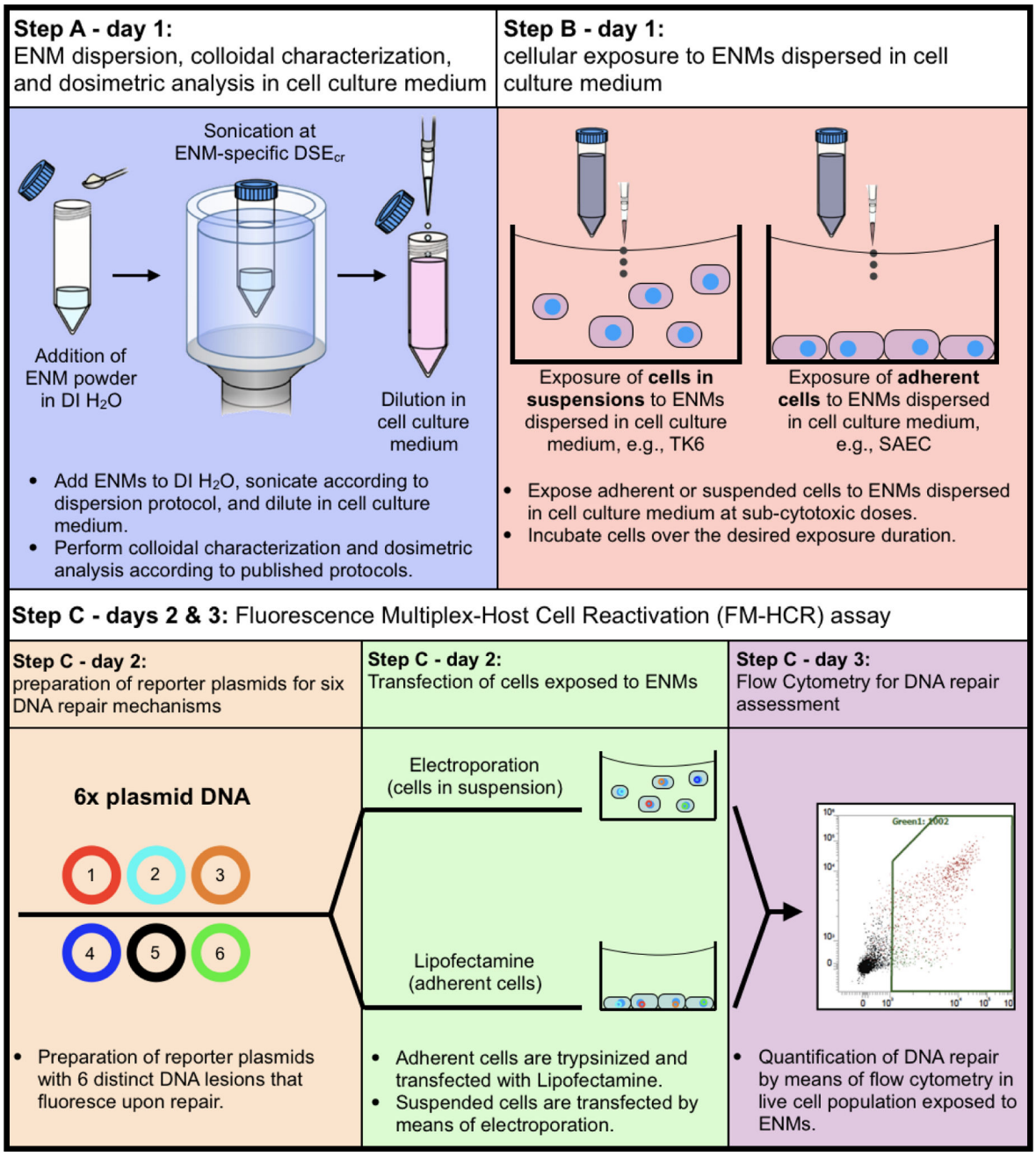

Figure 1. Protocol overview for assessing DNA repair capacity of cells using the Fluorescence Multiplex Host Cell Reactivation (FM-HCR) assay.

A. Engineered nanomaterials are suspended in cell culture medium according to the dispersion preparation protocol by Cohen *et al.*[43] **B.** Cells are exposed at the desired ENM concentration over the desired duration of time. **C.** Fluorescence Multiplex-Host Cell Reactivation Assay. **Step I:** Reporter plasmids that carry specific DNA lesions are prepared. **Step II:** Reporter plasmids are then transfected to ENM-exposed cells by means of electroporation (for suspended TK6 cells) or lipofectamine (for adherent SAEC). **Step III:**

Author Manuscript Author Manuscript Author Manuscript Author Manuscript

The capacity of cells to repair the DNA lesions carried by the reporter plasmids corresponds to the production of fluorescent proteins and can be directly quantified using flow cytometry.

Author Manuscript Author Manuscript Author Manuscript Author Manuscript

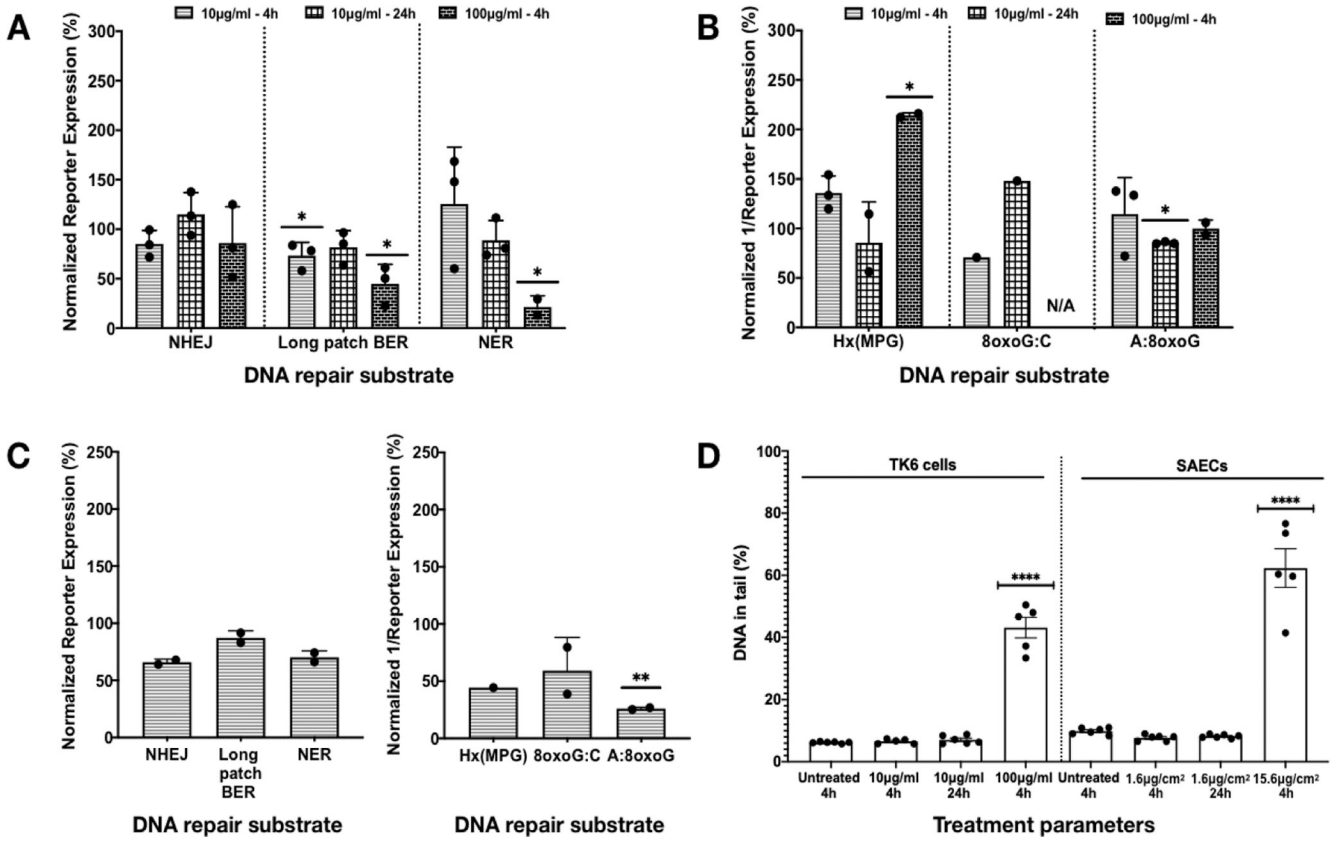

Figure 2. DNA damage and DRC quantification in SAEC and TK6 calls exposed to ZnO ENM.

A and B. DRC presented as reporter expression in TK6 cells exposed to ZnO ENM at various administered concentrations and time-points. Lesion-specific plasmid substrates are presented on the *x* axis for NHEJ, long patch BER, NER (A) and Hx(MPG), 8oxoG:C, and A:8oxoG (B). Reporter expression on the *y* axis is normalized to untreated control. Error bars represents mean ± SD; each dot represents one replicate. **C.** DRC presented as reporter expression in SAEC exposed to ZnO ENMs at various doses (presented as deposited ENM mass per cell surface area). *x* axis presents lesion-specific plasmid substrates and *y* axis presents reporter expression (%). **D.** Quantitation of DNA damage as % DNA in tail region for SAEC and TK6 cells following 4-hour exposures to ZnO ENM. Each dot represents approximately 250 cells. N/A: insufficient positive events; error bars: mean ± standard error (SE); experimental groups are compared for statistical significance to the untreated control; * $p<0.05$; ** $p<0.005$; *** $p<0.0005$; **** $p<0.00005$. Doses for SAEC: 1.6 µg/cm^2 at 4 and 24 hours hours correspond 8 µg/mL administered dose; 15.6 µg/cm^2 at 24 hours corresponds to 79 µg/mL administered dose. Doses for TK6 cells correspond to administered concentrations.

Author Manuscript Author Manuscript Author Manuscript Author Manuscript

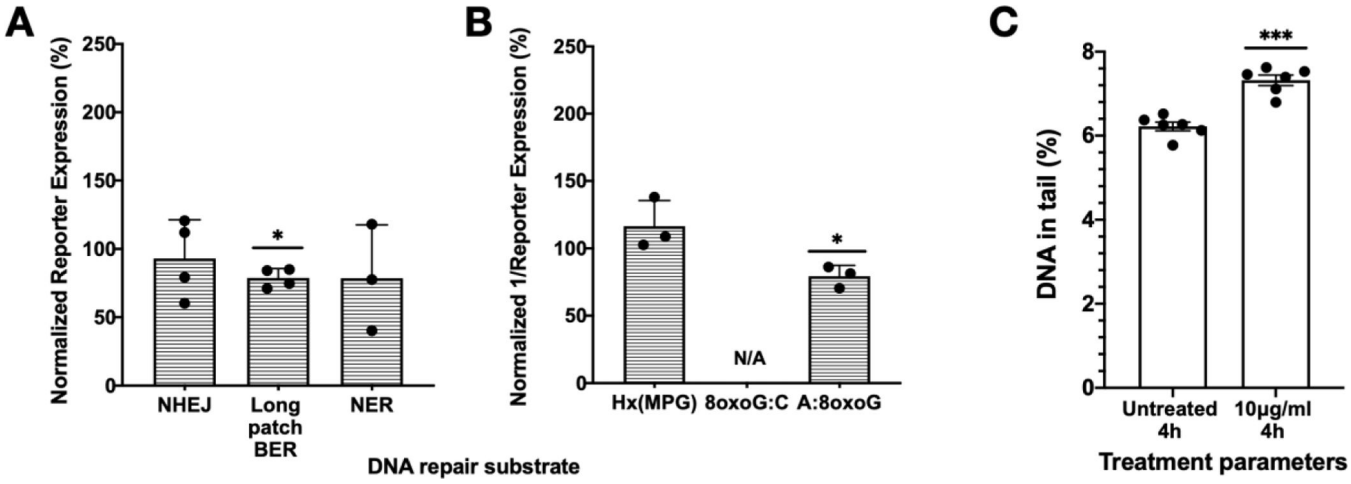

Figure 3. DNA damage and DRC quantification in TK6 cells exposed to CuO ENM.

A. DRC presented as reporter expression in TK6 cells exposed to CuO ENMs at 10 μg/ml (administered concentration) after a 4-h exposure. Lesion-specific plasmid substrates are presented on the x axis for NHEJ, long patch BER, NER (A) and Hx(MPG), 8oxoG:C, and A:8oxoG (B). Reporter expression on the *y* axis is normalized to untreated control. Error bars represents mean ± SD; each dot represents one replicate. **C.** Quantitation of DNA damage as % DNA in tail region for TK6 cells following a 4-hour exposure to CuO ENM. Each dot represents approximately 250 cells. Error bars represents mean ± standard error (SE); experimental groups are compared for statistical significance to the untreated control; * $p<0.05$; ** $p<0.005$; *** $p<0.0005$.

Author Manuscript
Author Manuscript
Author Manuscript
Author Manuscript

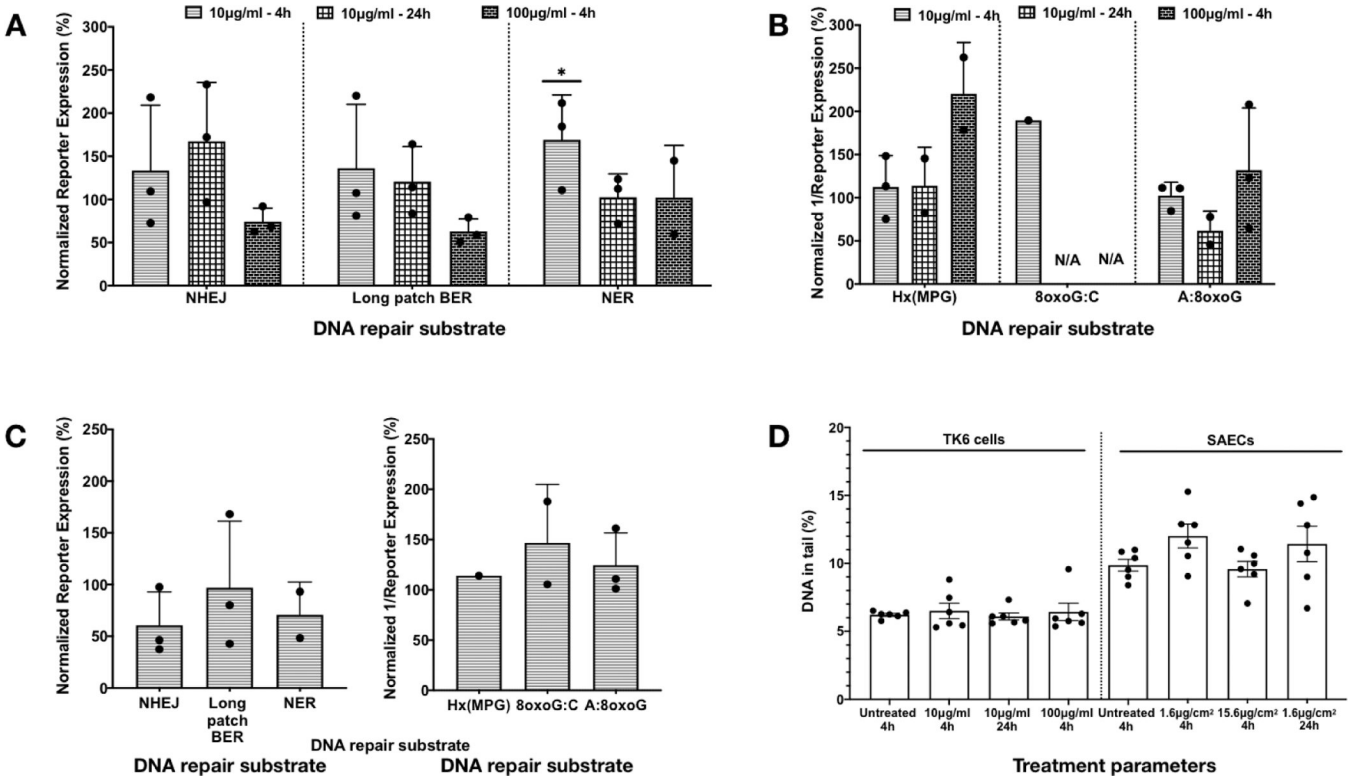

Figure 4. DNA damage and DRC quantification in SAEC and TK6 calls exposed to Ga_2O_3 ENM.

A and B. DRC presented as reporter expression in TK6 cells exposed to Ga_2O_3 ENMs at various administered concentrations and time-points. Lesion-specific plasmid substrates are presented on the *x* axis for NHEJ, long patch BER, NER (A) and Hx(MPG), 8oxoG:C, and A:8oxoG (B). Reporter expression on the *y* axis is normalized to untreated control. Error bars represents mean ± SD; each dot represents one replicate. **C.** DRC presented as reporter expression in SAEC exposed to Ga_2O_3 ENMs at various doses (presented as deposited ENM mass per cell surface area). *x* axis presents lesion-specific plasmid substrates and *y* axis presents reporter expression (%). **D.** Quantitation of DNA damage as % DNA in tail region for SAEC and TK6 cells following 4-hour exposures to Ga_2O_3 ENM. Each dot represents approximately 250 cells. N/A: insufficient positive events; error bars: mean ± standard error (SE); * $p<0.05$. Doses for SAEC: 1.6 µg/cm^2 at 4 and 24 hours hours correspond 5 µg/mL administered dose; 15.6 µg/cm^2 at 24 hours corresponds to 54 µg/mL administered dose. Doses for TK6 cells correspond to administered concentrations.

Author Manuscript Author Manuscript Author Manuscript Author Manuscript

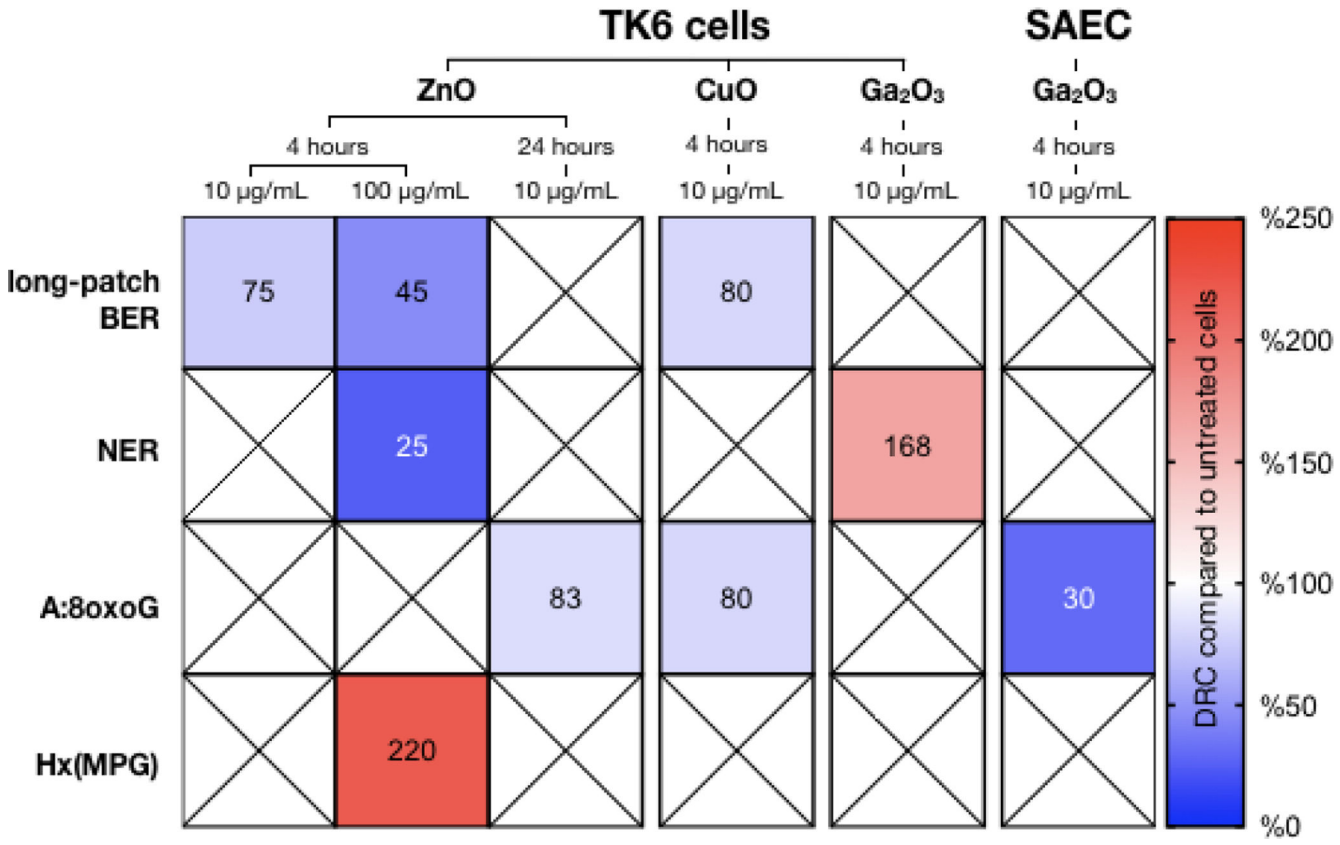

Figure 5: Overview of DNA repair capacity (DRC) changes following treatment of SAEC or TK6 cells with ZnO, CuO, or Ga_2O_3 ENM.

Baseline DRC from untreated cells is set at 100% (white color). Blue color denotes statistically significant DRC inhibition (<100%) while red color denotes statistically significant DRC increase compared to untreated cells. SAEC: small airway epithelial cells; BER: base-excision repair; NER: nucleotide excision repair; Hx(MPG): hypoxanthine methylpurine glycosylase; ×: non-significant change.

Author Manuscript Author Manuscript Author Manuscript Author Manuscript

Table 1.

Diseases and functional consequences possibly associated with inhibited or increased DNA repair activity

DNA repair pathway	Diseases possibly associated with DNA repair inhibition	Functional consequences possibly associated with increased DNA repair activity
BER (base excision repair)	neurodegeneration;[134] Alzheimer's disease;[135] complete defect in immunoglobulin class-switch recombination, hyper-immunoglobulin M syndrome, infections, lymphoid hyperplasia[136,137]	gastric,[138] colorectal,[139] and ovarian cancer[139]
NER (nucleotide excision repair)	Parkinson's disease;[140] increased genomic sensitivity to UV radiation[141]	ERCC1-associated resistance to platinum-based chemotherapy against gastric[142] and bladder cancer[143]
NHEJ (non-homologous end joining repair)	immunodeficiency[144]	hyperactive NHEJ promotes leukemia in the context of Fanconi anemia[145]
MPG (methylpurine-DNA glycosylase-mediated repair)	diabetes, ischemic heart disease[146]	lung cancer[147]
A:8oxoG (oxidative lesion repair initated by MUTYH DNA glycosylase)	atherosclerosis;[135] colon polyposis[136]	N/A
8oxoG:C (oxidative lesion repair initiated by OGG1 glycosylase)	lung cancer[147]	potential excess activation of OGG1-dependent transcription[148]

N/A: no relevant studies available in the literature at the time of writing

Author Manuscript

Author Manuscript

Author Manuscript

Author Manuscript

Table 2.

Physicochemical Characterization of ENMs Used in DNA Repair Assessment[a]

ENM	SSA (m^2/g)	d_{BET} (nm)	d_{TEM} (nm)
Ga_2O_3	251 ± 19	4	<5
CuO	[b] 14 ± 1	[b] 71	[b] 50 ± 11
ZnO	[b] 16 ± 1	[b] 61	[b] 46 ± 17

[a] SSA (specific surface area) as measured by nitrogen adsorption according to the Brunauer-Emmett-Teller (BET) method; d_{BET}, primary particle diameter calculated from SSA values; d_{XRD}, particle diameter as determined by X-ray diffraction.

[b] Data taken from Duean *et al.*[31]

Author Manuscript

Author Manuscript

Author Manuscript

Author Manuscript

Table 3.

Colloidal characterization of ENMs used in DNA repair assessment[a]

ENM	DI H_2O				RPMI			SAGM			
	d_H (nm)	PDI	ζ (mV)	DSE_{cr} (J/mL)	d_H (nm)	PDI	ζ (mV)	d_H (nm)	PDI	ζ (mV)	ρ_{eff} (g/mL)
Ga_2O_3	94 ± 3	0.201	38 ± 1	76	400 ± 9	0.329	−6 ± 0	2027 ± 245	0.417	−11 ± 1	1.13 ± 0.01
CuO	434 ± 22	0.330	−14 ± 0	416	434 ± 22	0.111	−12 ± 2	702 ± 184	0.686	−9 ± 1	6.153 *
ZnO	274 ± 6	0.188	18 ± 1	420	849 ± 75	0.444	−12 ± 2	301 ± 6	0.235	−9 ± 0	6.155 *

[a] d_H, hydrodynamic diameter as measured by dynamic light scattering (DLS); PDI, polydispersity index associated with intensity-weighted DLS measurements; ζ, zeta-potential measured by electrophoretic light scattering; DSE_{cr}, critical delivered sonication energy as measured by a protocol we have previously provided elsewhere;[86] ρ_{eff}, effective density as measured by the Harvard volumetric centrifugation method;[88]

* density values as measured by N_2 pycnometer and reported elsewhere were used as ρ_{eff} for ZnO and CuO ENMs due to their lack of agglomeration in SAGM.

Author Manuscript Author Manuscript Author Manuscript Author Manuscript

Table 4.
Composition of plasmid cocktails used in this study.

Three plasmid cocktails (Undamaged 1 & 2, Damage 1, and Damage 2) of 4 colors (BFP, GFP, mOrange, and mPlum) were prepared to measure repair capacity of cells for 6 DNA repair proteins/pathways. pmax backbone plasmid was used for this study. Details of plasmid fluorochrome reporter, filter, and flow channel were used to gate the fluorescent reporter events. The amount (in ng) of each plasmid reporting for a particular pathway of interest is mentioned. pmax_mOrange (in cocktail Damage 1) and pmax_BFP (in cocktail Damage 2) were used as transfection controls.

Serial #	Fluorochrome of reporter plasmid, fluorochrome, filter, flow channel	Undamaged cocktails 1 & 2		Damage cocktail 1			Damage cocktail 2		
		Plasmid	Amount (ng)	Plasmid	Amount (ng)	Pathway	Plasmid	Amount (ng)	Pathway
1	**BFP** (Pacific Blue, 440/50, VL-1)	pmax_BFP	50	pmax_BFP_ScaI digested	100	NHEJ	pmax_BFP	25	Control
2	**GFP** (FITC, 530/30, BL-1)	pmax_GFP	50	pmax_GFP_THF	50	Long patch BER	pmax_GFP_Hx	50	Hx(MPG)
3	**mOrange** (Phycoerythrin/PE, 585/16, YL-1)	pmax_mOrange	100	pmax_mOrange	100	control	pmax_mOrange_8oxoG-C	100	8oxoG:C
4	**mPlum** (PE-Cy5.5, 695/40, YL-3)	pmax_mPlum	100	pmax_mPlum_UV800J/m^2	100	NER	pmax_mPlum_A-8oxoG	100	A:8oxoG
5	-	pcx_nnx-D3GFP	1000	pcx_nnx-D3GFP	1000	Carrier	pcx_nnx-D3GFP	1000	Carrier